



DOCTORATE IN APPLIED ELECTRONICS

RESEARCH THEME: BIOMATERIALS

*THESIS TITLE: SYNTHESIS AND CHARACTERIZATION
OF NOVEL BIOMATERIAL SURFACES DECORATED
WITH CHITOSAN DERIVATIVES*

(XXX of Doctorate Cycle)

PhD student

Sofia Concolato

Tutor

Prof. Monica Orsini

The work described in this Ph.D. thesis was partially performed at LASS (Laboratorio Analisi di Superfici) – Roma Tre University.

Abstract

New strategies of functionalization of poly(ϵ -caprolactone) (PCL), titanium and Ti6Al4V alloy with biomolecules were studied to improve the biocompatibility of these materials, used in many medical applications.

Poly(ϵ -caprolactone) (PCL) surface was activated *via* alkaline hydrolysis and subsequently lactose-modified chitosan (chitlac) was immobilized. Two kinds of chitlac, characterized by a different degree of derivatization of chitosan (respectively 64% and 9%) were synthesized and grafted to the activated PCL surface. Each step of the functionalization was investigated by a very sensitive surface technique, the Time of Flight Secondary Ion Mass Spectrometry (ToF-SIMS), coupling with univariate and multivariate statistical analysis. The results showed the formation of a homogeneous layer of chitlac on the hydrolyzed PCL.

Covalent grafting of chitosan on titanium and Ti6Al4V alloy was performed to improve biocompatibility, in terms of antibacterial properties. In detail, the chitosan was anchored to the metal surface, which was previously activated by carboxyl groups. Different pretreatments of the surface were studied, to identify the one, which could permit the highest functionalization efficiency of chitosan. The carboxylation of metal surfaces and the subsequent grafting with chitosan were analyzed by Fourier Transform Infrared Spectroscopy (FTIR) and X-ray Photoelectron Spectroscopy (XPS). Also an electrochemical technique, the cyclic voltammetry was employed to confirm the grafting of chitosan on metal surfaces and to evaluate the stability of immobilization procedure.

Summary

Abstract	3
1. Introduction	6
1.1 Biomaterials.....	6
1.2 Polymers	8
1.3 Metals	11
1.4 Functionalization of biomaterials	16
1.5 The chitosan in biomedical applications	21
1.6 Functionalization of poly(ϵ -caprolactone) for biomedical applications.....	24
1.7 Functionalization of titanium and its alloys surface for biomedical applications	26
1.8 References	29
2. Aim of the thesis	35
3. Functionalization of poly(ϵ-caprolactone) surface with lactose-modified chitosan via alkaline hydrolysis.....	36
3.1. MATERIALS	38
3.1.1 Synthesis of lactosylated chitosan (chitlac)	38
3.1.2 Preparation of PCL films by casting technique	38
3.1.3 Base-catalyzed hydrolysis treatment of the PCL film surface.....	39
3.1.4 Immobilization of chitlacA and chitlacB on the PCL film.....	39
3.2 METHODS.....	40
3.2.1 Scanning electron microscopy (SEM) characterization	40
3.2.2 ToF-SIMS characterization	40
3.2.3 Statistical data analysis	41
3.3 RESULTS AND DISCUSSIONS	41
3.3.1 SEM characterization.....	41
3.3.2 ToF-SIMS reference spectra from PCL membrane, chitosan and chitlac	42
3.3.3 Effects of hydrolysis treatment on PCL membrane.....	44
3.3.4 Evaluation of the degree of derivatization of chitlac	45
3.3.5 ToF-SIMS characterization of the chitlac grafting on PCL.....	46
3.3.6 Evaluation of grafting yield of chitlac A and B.....	50
3. 4 CONCLUSIONS	51
3.5 REFERENCES	52

4. Functionalization of titanium and Ti6Al4V substrate with chitosan by carboxyl groups as linker agent	54
4.1 MATERIALS	55
4.1.1 Preliminary preparation of substrates	55
4.1.2 Substrate Pretreatments	55
4.1.3 Carboxylation of titanium and Ti6Al4V alloy surface	56
4.1.4 Grafting of chitosan on carboxylated samples.....	56
4.1.5 Chitosan physisorbtion on titanium and Ti6Al4V alloy.....	56
4.2 METHODS.....	57
4.2.1 Scanning electron microscope (SEM)	57
4.2.2 Fourier Transform Infrared Spectrometry (FTIR-ATR).....	57
4.2.3 X-ray Photoelectron Spectroscopy (XPS) characterization.....	57
4.2.4 Cyclic voltammetry characterization	58
4.3 RESULTS AND DISCUSSIONS	58
4.3.1 SEM characterization: study of the effect of HCl and HF etching treatments on titanium and Ti6Al4V surfaces	58
4.3.2 FTIR-ATR analysis	61
4.3.2.1 Carboxylation of titanium surfaces	61
4.3.2.2 Chitosan grafting on carboxylated titanium surface	63
4.3.2.3 Carboxylation of Ti6Al4V surfaces	66
4.3.2.4 Chitosan grafting on the carboxylated Ti6Al4V surface	68
4.3.3 X-ray Photoelectron Spectroscopy (XPS) analysis	70
4.4.3.1 Carboxylation and chitosan grafting on titanium surfaces.....	71
4.4.3.2 Carboxylation and chitosan grafting on Ti6Al4V surfaces	72
4.3.4 Electrochemical analysis: cyclic voltammetry	74
4.4 CONCLUSIONS	78
4.5 REFERENCES	79
5. Conclusions	81

Chapter 1

Introduction

1.1 Biomaterials

The current definition of biomaterial is a “material intended to interface with biological systems to evaluate, treat, augment or replace any tissue, organ or function of the body” [1].

Biomaterials in the form of implants (sutures, joint replacements, bone plates, etc.) and medical devices (artificial hearts, pacemakers, blood tubes, etc.) are widely used to replace and restore the function of traumatized or degenerated tissues or organs, and thus improve the quality of life of the patients [2].

The worldwide biomaterials market is valued at close to \$24,000M. Orthopaedic and dental applications represent approximately 55% of the total biomaterials market. Orthopaedics products worldwide exceeded \$13 billion in 2000, an increase of 12% over 1999 revenues. Expansion in these areas is expected to continue due to number of factors, including the ageing population, an increasing preference by younger to middle aged candidates to undertake surgery, improvements in the technology and life style, a better understanding of body functionality, improved aesthetics and need for better function [3].

The first and most important requirement for the choice of the biomaterial is its acceptability by the human body, its biocompatibility [4]. It is defined as the ability of a material to perform with an appropriate host response in a specific application. A biomaterial must be non-toxic, because it must not adversely affect the local and systemic host environment of interaction (bone, soft tissues, blood, as well as intra and extracellular fluids). It's likewise important, a biomaterial must be functional and it must engage in an appropriate response with the body, and it can fulfil its purpose.

In terms of the tissue response to the implant surface, biomaterials can be divided in three categories: bioinert, bioresorbable and bioactive biomaterials.

The term bioinert refers to any material that once inserted in the human body has minimal interaction with its surrounding tissue. Usually, the most common response of tissues to these materials is the formation of a non-adherent fibrous capsule, that “walls-off” or isolates the implant from the host. This leads to a complete encapsulation of the implant within the fibrous layer, as

shown in figure 1.1(a). Examples of these biomaterials are stainless steel, titanium, alumina, partially stabilised zirconia, and ultra high molecular weight polyethylene [5].

The term bioactive, instead, refers to materials, which once incorporated in the body, over time, actively interact with cells to achieve a better outcome. For example, an implant produces chemical bonds with bone tissues, in a process called osseointegration. In this context, synthetic hydroxyapatite [$\text{Ca}_{10}(\text{PO}_4)_6(\text{OH})_2$] coatings applying on an implant surface, such as titanium, offer several biological advantages such as the stimulation of bone formation and the bonding acceleration between the implant surface and surrounding tissues, as shown in figure 1.1(b) [6]. Other examples of bioactive materials are the glass ceramic and the bioglass (figure 1.1(c)).

In the end, the term bioresorbable, refers to any material that upon placement within the human body starts to degrade and slowly replaced by advancing tissue (such as bone). The necessary requirement for these materials, is that the degradation products could be tolerated by the body. Examples of these biomaterials are the tricalcium phosphate [$\text{Ca}_3(\text{PO}_4)_2$] (figure 1.1(d)) and many aliphatic polyesters, such as the poly(lactic acid) (PLA) and the poly(ϵ -caprolactone) (PCL). Other examples include also natural biopolymers as dextran, chitosan, hyaluronic acid and alginates, which can be obtained from microbial, animal, and vegetal sources [7].

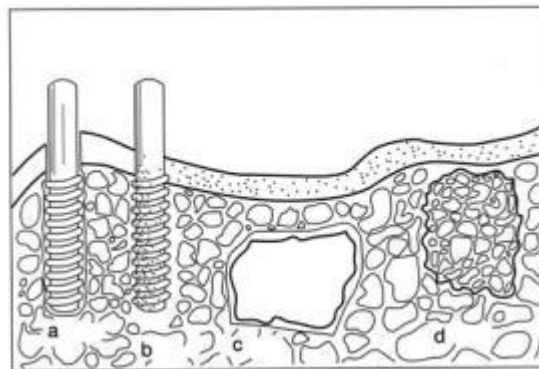


Figure 1.1: Classification of biomaterials according to their bioactivity (a) bioinert alumina dental implant, (b) bioactive hydroxyapatite [$\text{Ca}_{10}(\text{PO}_4)_6(\text{OH})_2$] coating on a metallic dental implant, (c) surface active bioglass and (d) bioresorbable tricalcium phosphate implant.

The most common classes of materials used as biomedical materials are metals, polymers, ceramics, and composites. Between them, metals and polymers have aroused me interest for my studies and they are presented in detail, in the next sections.

Ceramics are used in several different fields such as dentistry, orthopedics, and as medical sensors. Overall, however, these biomaterials have been used less extensively than either metals or polymers. The major drawbacks to the use of ceramics and glasses as implants are their brittleness

and poor tensile properties. Among biomedical ceramics, alumina has the highest mechanical properties, but its tensile properties are still below those of metallic biomaterials.

Composites are engineering materials that contain two or more materials that have different physical properties with an interface separating them. These materials consist of mixtures of polymers, metals and ceramics to form materials such as fiberglass, a mixture of glass fibers coated with a polymeric matrix. In recent years, scientific research tends to develop biomedical composite materials because of these materials present new alternative solutions for load-bearing tissue components.

1.2 Polymers

Polymers range from familiar synthetic plastics such as polystyrene to natural biopolymers such as DNA and proteins that are fundamental to biological structure and function. Because of their broad range of properties, both synthetic and natural polymers play an essential and ubiquitous role in everyday life.

The large molecular mass of polymers relative to small molecule compounds produces unique physical properties, including toughness, viscoelasticity, and a tendency to form glasses and semicrystalline structures rather than crystals [8].

The mechanical and thermal behaviour of polymers is influenced by several factors, including the composition of the backbone, chemical side groups, chain structures and different molecular weight [9]. Changes in polymer composition or structure increase resistance to relative chain movement, so this resistance increases the strength and decreases the plasticity of the material. Substitutions into the backbone increase its rigidity limiting the chain movement.

Polymers are attractive materials for biomedical applications such as cardiovascular devices, replacement and proliferation of various soft tissues. They are also used in drug delivery systems, diagnostic supports and as a reconstructive material for tissue engineering. The current applications of them include cardiac valves, artificial hearts, vascular grafts, breast prosthesis, contact and intraocular lenses, dialysis systems, coating materials for medical products, surgical materials etc.

The main advantages of the polymeric biomaterials compared to metal or ceramic materials are ease of manufacturability to produce various shapes (latex, film, sheet, fibers, etc.), ease of secondary processability, reasonable cost, and availability with desired mechanical and physical properties. [10].

Polymers may be durable or biodegradable. Non-biodegradable polymers do not undergo any chemical change in vivo and they are used in a wide range of biomedical applications that require long-term structural stability in order to replace soft tissues, such as cartilage, vessel wall, lens, tendon and skin. Some of these polymers are: polyurethane (PE), polymethylmethacrylate (PMMA) and poly(ethylene terephthalate) (PET).

In recent years, advances of innovative technologies in tissue engineering, regenerative medicine, gene therapy and drug delivery systems have been promoted through the use of biodegradable polymers. Biodegradable polymers contain functional groups that may be cleaved in vivo, leading to the fragmentation of the polymeric chains and therefore its solubilization. The success of these class of polymers is due to two major advantages that non-biodegradable biomaterials do not have. First, they do not elicit permanent chronic foreign-body reactions due to the fact that they are gradually absorbed by the human body and do not permanently leave traces of residual in the implantation sites, unlike the metals. Second, some of them have been recently applied to the tissue engineering concerning with the repair and regeneration of lost or damaged tissues and organs, thanks to the interaction of their biodegradation with immunologic cells like macrophages. Hence, surgical implants made from biodegradable biomaterials could be used as a temporary scaffold for tissue regeneration.

In detail, biodegradable polymers can be classified in biological and synthetic derived polymers. Naturally derived polymers have the potential advantage of supporting cell adhesion and function. In natural polymers, cellulose, alginate, chitosan, hyaluronic acid and genetic materials such as DNA or RNA, can be included. They have many advantages including biodegradability, cytocompatibility, and unique physical, chemical, and mechanical properties. They offer cell recognition sites necessary for cell adhesion and proliferation. However, concerns over the complex structural composition of natural polymers, as well as immunogenicity and pathogen transmission, have driven the development of synthetic polymers. Nowadays, synthetic materials have become attractive alternative materials for biomedical applications: they usually have controlled structure, a higher degree of processing flexibility, and no immunological concerns. To achieve the specific properties, properly designed synthetic polymers require further modifications without altering the bulk properties [11].

Aliphatic polyesters, such as polyglycolide (PGA), polylactide (PLA), their copolymers (PLGA) and poly(ϵ -caprolactone) (PCL), polyanhydrides and aliphatic polycarbonates, such as poly(trimethylene carbonate) (PTMC), are only some of the examples of biodegradable synthetic

polymers, used in biomedical applications. Among them, my study will be focus on the poly(ϵ -caprolactone).

Poly(ϵ -caprolactone) (PCL) was one of the earliest polymers synthesized by the Carothers group in the early 1930s [12]. It became commercially available following efforts to identify synthetic polymers that could be degraded by microorganisms. Generally, PCL can be prepared by ring-opening polymerization of ϵ -caprolactone using a variety of anionic, cationic and co-ordination catalysts (figure 1.2) [13].

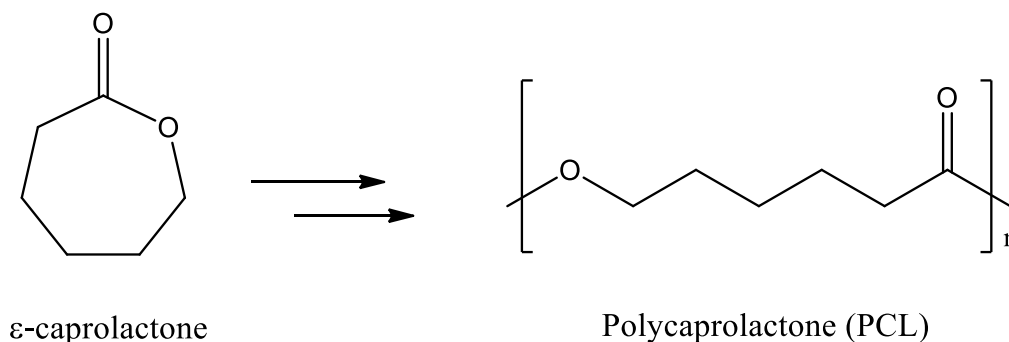


Figure 1.2: Poly(ϵ -caprolactone)

PCL is a semicrystalline polyester; its crystallinity tends to decrease with increasing molecular weight. It is hydrophobic, with a melting temperature of 55 – 60 °C and glass transition temperature of –54 °C and it has a good organic solvent solubility.

PCL has low tensile strength (~23 MPa), but very high elongation at breakage (4700%) making it a very good elastic biomaterial. As a consequence, PCL may be processed to obtain various material shapes, such as microspheres, fibers and porous materials, and therefore it is used as wound closure staples, scaffolds or long-term drug delivery systems, such as one-year implantable contraceptive.

In particular, *in vivo*, the favor as a long-term implant delivery device is due to very low degradation rate and high drug permeability [14]. In current research, PCL is used for the development of micro- and nano-sized drug delivery vehicles, but the degradation rate (2–3 years) is a significant issue to be approved by Food and Drug Administration (FDA) for this use. PCL is often blended or copolymerized with other polymers to expedite overall polymer erosion.

On the other hand, tissue engineering implications of PCL are numerous. PCL and PCL composites have been used as tissue engineering scaffolds for regeneration of bone, ligament, cartilage, skin, nerve, and vascular tissues.

PCL's processability allows for the formation of scaffolds composed of adhered microspheres, electrospun fibers, or through porous networks produced by porogen leaching.

However, the use of PCL is limited by its high hydrophobicity which leads to unfavorable cell adhesion, spreading and proliferation. Therefore, functional modification of PCL is required. [15]

1.3 Metals

Throughout the history, metals have played a fundamental role in enabling technological development. The use of metallic materials for medical implants can be traced back to the 19th century, leading up to the era when the metal industry began to expand during the Industrial Revolution. The development of metallic implants was primarily driven by the demands for approaches to bone repair, typically internal fracture fixation of long bones. However, almost no attempts of implanting metallic devices were successful until Lister's aseptic surgical technique was implemented in the 1860s [16].

Since then, metallic materials have predominated in orthopedic surgery, playing a major role in most orthopedic devices, including temporary devices (e.g. bone plates, pins and screws) and permanent implants (e.g. total joint replacements). Concurrently, metals also found applications in dental and orthodontic practice. Nowadays, metallic biomaterials have become a multi-billion dollar industry with millions of procedures performed to date.

The metals used as biomaterials are iron (Fe), chromium (Cr), cobalt (Co), nickel (Ni), titanium (Ti), tantalum (Ta), molybdenum (Mo), and tungsten (W) and their alloys as the stainless steels, the cobalt-chromium alloy and titanium-based alloys.

All metallic elements are crystalline solids. The structure of all crystals can be described in terms of a lattice, with a group of atoms attached to every lattice point. The lattice is divided into a number of identical blocks, or unit cells. The French scientist Auguste Bravais demonstrated in 1850 that only these 14 types of unit cells are compatible with the orderly arrangements of atoms found in crystals, in three dimensions.

The lattices listed by Bravais are divided into six or seven major crystal symmetry systems, as reported in figure 1.3.

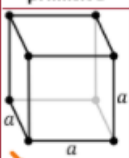
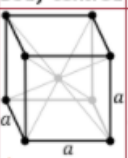
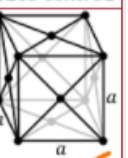
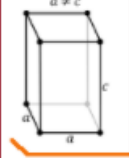
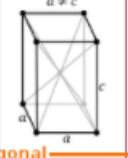
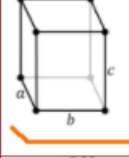
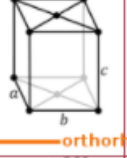
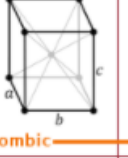
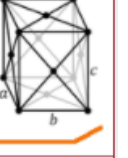
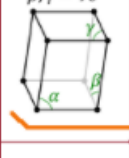
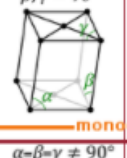

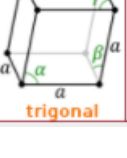
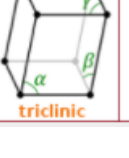
primitive	side-centred	body-centred	face-centred
			
cubic			
			
tetragonal			
			
orthorhombic			
			
monoclinic			
			
hexagonal	trigonal	triclinic	

Figure 1.3: Bravais lattices in three dimensions

In all the cases the unit cell represents a parallelepiped. Conventionally, the lattice vectors are named \underline{a} , \underline{b} and \underline{c} and the angles are given by the Greek letter, *i.e.* the angle between \underline{a} and \underline{c} is β [17].

The relationship between the sides and the angles determines the crystal system.

Metallic biomaterials used for implant production have either close-packed atomic structures with face-centered cubic (FCC) or hexagonal close-packed (HCP) unit cells or nearly close-packed structures forming body-centered cubic (BCC) structures. Nevertheless, the most of metal crystals, in contrast to these ideal atom arrangements, contains lattice defects such as vacancies, dislocations, grain boundaries etc. The presence of point, line and planary defects in metal internal structure has a strong effect on mechanical, physical and chemical properties.

Metals tend to have high tensile strengths and good fatigue resistance compared to ceramics and polymers. This means that a metallic implant will require a high load to cause deformation and will resist failure caused by repeated loadings. Perhaps most importantly in biological applications, metals are not prone to brittle fracture. That is, metals will deform before failing and not suddenly

break. Moreover, their electrical properties, as conductivity, permit to use them, as electrodes in implantable cardiac pacemakers and defibrillators.

In general, metals exhibit properties that make them attractive for load-bearing applications, but it is not easy the choice of particular metal for a given application. Metals have different mechanical properties which make some advantageous compared with others for certain situations, and even metals with identical compositions can behave differently depending on how they are processed. However, for biological applications, the reaction of the metal with the physiological environment needs to be considered.

The physiological environment is at 37 °C aqueous solution containing dissolved gases, electrolytes, proteins, and cells. In fact, it is similar warm sea water, which can corrode many metals. By corrosion, potentially harmful metal ions can be released into the body and could compromise the mechanical integrity of the implant. For these reasons, corrosion resistance is imperative when choosing a metal.

In addition to corrosion, toxicity also needs to be considered. Aluminium, for example, has excellent mechanical properties, but has been associated with toxicity if excessive amounts of it accumulate in the body.

The final consideration for choosing a metal for a medical implant is cost. Some metals cost much more than others as a raw material, and processing and machining costs can vary considerably depending on application.

It is worthwhile to remember that most metals are not used in their elemental form, but rather alloyed or mixed with other metals, because alloys frequently provide improvement in material properties, such as strength and corrosion resistance.

Stainless steel has high strength, chemical inertness and resistance to corrosion due to the presence of chromium (Cr) [18]. In medical applications, typical medical grade of stainless steel is the 316L, which is predominantly iron alloyed with major amounts of chromium and nickel. The main disadvantage of 316L is the presence of nickel. Indeed, Ni has generally a poor biocompatibility. Stainless steels are used in bone plates, spinal fixation, screws, and hip and knee components.

Cobalt-based alloys possess good wear resistance and fatigue strength. Thus, they are used as prosthesis stems, load-bearing components in joint replacement devices and dentistry castings.

Other examples are magnesium-based alloys, tantalum-based alloys, niobium-based alloys and precious alloy such as gold-based alloys and silver-based containing a large amount of platinum and gold.

Among metals and alloys used as biomaterials, titanium and its alloys are extensively employed.

Indeed, they are today's equipments for orthopedic, dental and cardiovascular surgeons. In orthopedics, titanium is used as plates, pins, fixing screws for bone fractures [19]. Titanium alloys are also used as various components for total hip prostheses and as femoral and tibia components in total knee arthroplasty. Ti alloys due to the combination of its excellent characteristics such as high strength, low density, high specific strength, good resistance to corrosion, complete inertness to body environment, enhanced biocompatibility, moderate elastic modulus of approximately 110 GPa are a suitable choice for implantation.

However, even though titanium is the fourth most abundant element in the Earth's crust, the cost of titanium is high due to its high melting point and extreme reactivity. The high cost includes both the "mill operations" (extraction, ingot melting, and primary working) as well as many of the secondary operations conducted by the user.

In addition to above properties different crystal structures of titanium allow manipulation by heat treatments to produce different types of alloy microstructures to suit the required mechanical properties.

The crystal structure of pure titanium at ambient temperature and pressure is HCP (close-packed hexagonal) α phase with a c/a ratio of 1.587. At about 890°C, the titanium undergoes an allotropic transformation to a BCC (body-centered cubic) β phase which remains stable to the melting temperature [20].

The selective addition of alloying elements to titanium enables a wide range of physical and mechanical properties to be obtained. Some alloying elements raise the alpha-to-beta transition temperature (alpha stabilizers) while others lower the transition temperature (beta stabilizers). Aluminum, gallium, germanium, carbon, oxygen and nitrogen are alpha stabilizers. Aluminum, the principal alpha stabilizer, increases tensile strength, creep strength, and elastic module.

Molybdenum, vanadium, tantalum, niobium, manganese, iron, chromium, cobalt, nickel, copper and silicon are beta stabilizers.

Some elements notably tin and zirconium behave as neutral solutes in titanium and have little effect on the transformation temperature [21-22].

Titanium alloys are classified according to the amount of alpha and beta phases retained in their structures at room temperature [23]. Classifications include commercially pure, alpha and near-alpha, alpha-beta, and beta. The commercially pure titanium (CP) and alpha alloys have essentially all-alpha microstructures. Beta alloys have largely all-beta microstructures after air cooling from the solution treating temperature above the beta transus. Alpha-beta alloys contain a mixture of alpha and beta phases at room temperature.

Commercially pure or unalloyed titanium typically contains between 99%-99.5% titanium, with the balance being made up of iron (as a main element) and the interstitial impurity elements hydrogen, nitrogen, carbon, and oxygen. In the alloys of titanium, Fe and O content determine the grade and strength; the C, N and H are present as impurities and in the higher-strength grades, oxygen and iron are intentionally added to the residual amounts.

Alpha & Beta Alloys are metastable and contain both alpha stabilizers and beta stabilizers. α stabilizers are used to give strength with 4-6% and β stabilizers are used to allow the β phase to retain at room temperature. The alloy microstructure depends on chemical composition, processing history and heat treatment.

In particular, Ti6Al4V is the main $\alpha + \beta$ Ti alloy used in biomedical applications. The main alloying elements are aluminum (5.5–6.5%) and vanadium (3.5–4.5%) [24]. This alloy is used to obtain biomaterials with higher strengths than commercial pure titanium but with the same corrosion resistance and osseointegration properties. Its fatigue strength depends strongly on the size and distribution of the $\alpha + \beta$ phase regions. Due to its excellent corrosion resistance, Ti6Al4V is also used as porous-coated or surface-textured orthopedic implants.

Although titanium and its alloys are characterized by excellent mechanical properties and biocompatibility with human tissue, titanium-based surgical implantation is still associated with certain clinical challenges. Indeed, its biocompatibility is often not sufficient to attain true and complete adhesion between the implant and the tissue.

The titanium has an inert behaviour, so the body tries to encapsulate the Ti-implant. Furthermore, it does not bond directly to the surrounding tissues, resulting in micromovements and eventually loosening of the implant. [25]. For example, the statistics show that 25% of hip replacement surgeries and about the 10-15% of dental implant surgeries are revised due to previous implant failure.

On the other end, according to previous studies, the implant surface itself represents a preferential site for bacterial adhesion [26].

Therefore, it is imperative to design alloy surfaces to facilitate osseointegration and mitigate adverse tissue response such as foreign body reactions and infection. In this context, the surface modification plays a key role in tailoring the surface of biomaterials to allow better adaptation to the physiological surroundings and deliver the required clinical performance.

1.4 Functionalization of biomaterials

Biocompatibility, biomaterials-tissues interactions and bacterial adhesion represent the most important factors to consider for the success of implants in the human body.

Despite the various advancements made, incomplete understanding of the interactions between biomaterials and biological tissues still limits the advancement in clinical settings.

The surface of biomaterials plays a key role in the performance of the biomaterials. It is well known that cellular interactions with biomaterials are of fundamental importance in many normal and pathological biological processes. Nevertheless, specific and complex mechanisms govern the reactions that occur at the interface between the biomaterial and the cellular environment [27]. Schematically, figure 1.4 describes the starting interactions between biomaterials and cells. These interactions are governed by surface energy, chemical composition, stiffness, as well as roughness and topography of the biomaterial surface in contact with the biological environment [28].

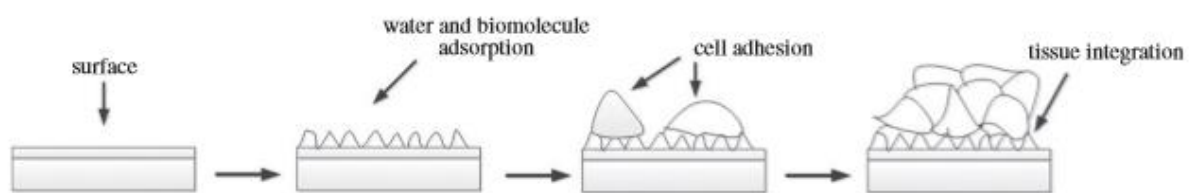


Figure 1.4: Interaction of cells with biomaterials

For these reasons, the surface functionalization is a research field that has received much attention although biomaterials as the metals and the polymers might possess excellent bulk properties [29]. Functionalization of biomaterials could thus be a pertinent solution to modulate the surface properties in order to endow currently available biomaterials with specific and desirable functions.

Surface functionalization is defined as any surface modification that changes a material's surface composition, structure, and morphology, leaving the bulk intact.

In this context, the aim of improving biocompatibility can be realized by the following surface treatments, which are schematically illustrated in figure 1.5 [30]:

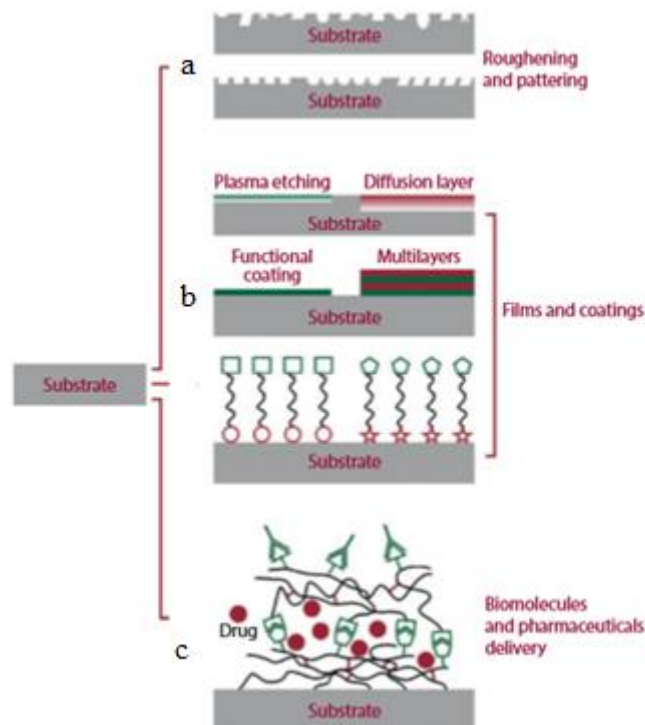


Figure 1.5: Surface functionalization methods.

a) Surface roughening methods and surface patterning

Mechanical methods of surface functionalization such as polishing, machining, grinding, and blasting are commonly used for metals surface modification, in order to obtain specific substrate topography, polish and roughen surface and enhance adhesion properties. Substrate roughening influences mainly the topology of the surface without causing any chemical changes. It results in significant increase of the surface area of the material and restriction of cell movement and contributes to the enhanced cell attachment.

Acid etching is one of the most popular chemical techniques to increase roughness for improving biocompatibility, in terms of osseointegration. Indeed, for example, smooth Ti implants have been reported to be less desirable for bone fixation than roughened ones because a rough Ti surface has shown better osteogenic activities such as cell attachment, cell proliferation and calcium deposition, proving to be beneficial for osseointegration [31].

Oxygen or argon plasma deposition is a very useful technique to alter the surface topography by occurrence of such processes as melting and recrystallization. This treatment leads to formation of more ridges and hydrophilic surface, compared to the original one. Nevertheless, in case of

polymeric materials, this technique leads to degradation of the polymer surface and changes in the top layer of the surface.

Surface patterning offers a more organized type of alteration from the original material. This widely used technique enables to obtain surfaces patterned in both micro and nanoscales and with different topography.

b) Surface films and coatings

Plasma etching, spin and dip coatings, layer by layer (LbL) films are some examples of the most common used techniques, meant for preparing thin films and coatings.

Plasma etching can also be applied prior to coating with another desired material, e.g., polymeric hydrogels and bioactive molecules. For example, grafting of different length biopolymer chains, subsequently after plasma pretreatment, can also alter the surface roughness.

Spin coating is a simple technique of thin films deposition on rotating at high speed flat substrate. Dip coating is another example of a straightforward method for obtaining thin films deposition by submerging in and withdrawing from a coating solution. In the case of dip coating, the uniformity of a film is difficult to control. Often these two techniques are applied after previous surface activation, e.g., plasma etching. Despite the disadvantages, these treatments are still used, for example, for the peptides attachment in orthopedic implants.

LbL strategy permits to obtain a nanostructured self-assembly films with different geometries, from simple two-dimensional multilayer films to complex three dimensional porous structure. The self-assembly mechanism is based on the electrostatic interactions. However, other types of interaction can also be used, as the hydrophobic interactions or hydrogen bonding.

c) Surface modification by biomolecules grafting

Properties as wear and corrosion resistance, chemical reactivity, hydrophilicity/hydrophobicity, blood compatibility, endothelialization, cell adhesion and growth, and antimicrobial, should be relevantly improved.

Some examples of the most common available techniques include chemical vapor deposition techniques (CVD), sol-gel treatment, self-assembled monolayers (SAMs) and grafting techniques.

CVD techniques are based on chemical reactions between chemical reagents in the gas phase and the substrate surface leading to the deposition of a nonvolatile coating on the substrate. In this context, plasma technology (plasma-enhanced CVD and plasma-assisted CVD), is a controllable and reproducible method that have been proven to be extremely efficient. It plays a key role in improving the metallic or polymeric surface properties such as biocompatibility, blood compatibility, cell adhesion and growth, wear and corrosion resistance, and controlled drug delivery. Surface properties may be thinly defined by varying the plasma parameters, tailored to produce different types of surfaces depending on the specific application and requirements [32].

Sol-gel treatment is used for the production of bioactive surface starting from a colloidal solution called sol. This sol acts as an integrated network of discrete particles or polymers network. This method, known for its simplicity, can provide molecular control over the incorporation and biological behaviour of the cells and proteins, for biomedical applications.

By SAMs technique, ordered organic films are created, directed through noncovalent interactions formed by the adsorption (chemisorption) of an active organic coating on a solid surface. A SAM is a properly organized layer of amphiphilic molecules with a “head group” at the end having special affinity for a substrate, on the other end of molecules a terminal functional group is present. This end functional group (tail groups) could be modulated, and generally properly chosen to improve hydrophilic and hydrophobic properties of the substrate [33].

Many procedures are reported in literature for the functionalization of biomaterial surfaces with bioactive molecules, as proteins and other biopolymers. These molecules have been introduced on the surfaces by two different adsorption or covalent linkages [18]. Biomolecules as biopolymers can be immobilized on appropriate surfaces using either a physisorption (chain attachment mainly through van der Waals interactions) or a covalent strategy (anchoring by chemical bonds). Biopolymer physisorption is a reversible process in which the chains with the sticking segments adsorb onto a suitable substrate. The release of biopolymers from such modified surfaces and the subsequent loss of activity potentially make them unsuitable for most biomedical applications. On the contrary, the covalent linkages allow a stable immobilization of the biomolecules on the biomaterial surface.

For this reason, it is important for biopolymers to be covalently immobilized on the surface. Many techniques for covalently bonding onto surfaces have been developed.

The covalent attachment of biopolymers can be obtained by an appropriate anchor (“grafting to”) on the surface. Otherwise the polymerization can be initiated from the surface (“grafting from”)

and the biopolymer is yielded in situ.

The “grafting to” method (Figure 1.6) involves reaction of (end)-functionalized polymer molecules with complementary functional groups located on the surface, resulting in the formation of tethered chains.

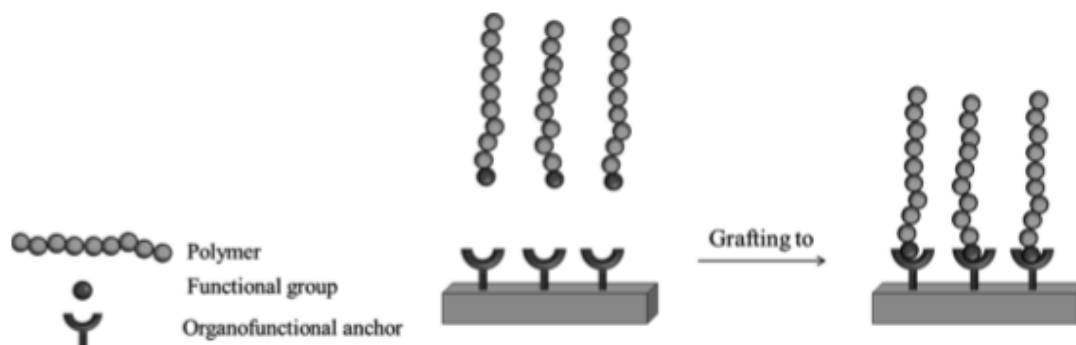


Figure 1.6 : "Grafting to" technique

For the attachment of these bioactive molecules, it is fundamental the functionalization of the substrate surface. Several methods can be used for initial surface functionalization or to immobilize anchors onto the solid surface, including electron beam-induced grafting, plasma treatment and ultraviolet (UV)-initiated photografting and various chemical treatments. In particular, by wet treatments, the surface activity can be modified by a chemical reaction with alkaline or acidic solution.

These wet treatments of polymeric surface by the aminolysis and the hydrolysis reactions, can bring about cleavages of the polymer main-chain bonds with following insertion of different functional groups on the surface.

Hydrolysis is a simple and frequently used method used to introduce the carboxyl group on the surface; however, it is pH dependent and might lead to unwanted degradation of the polymer surface. Aminolysis is a very simple reaction to introduce primary and secondary amine groups [34]. These surface treatments introduce functional groups on the polymer surface for a subsequent modification of biomaterial surfaces with biomolecules.

Using these methods, for example, a variety of polymer substrates ranging from conventional polymers, such as linear low-density polyethylene (LLDPE) and poly(ethylene terephthalate) (PET), to biodegradable poly(ϵ -caprolactone) (PCL) and poly(1,5-dioxepan-2-one) to silicone elastomers have been functionalized.

Also metals, as titanium, silver, gold, etc, can be functionalized by these approaches. For example, Falentin et al. reported the covalent anchoring of dispersin B and polyethylene glycol (PEG) onto stainless surfaces via the “grafting to” method in order to impart long-term durability to the coating and prevent biofilm formation when the stainless steel is aging [18].

Although “grafting to” was widely used in the early days due to the simplicity, there is a drawback that only a small amount of the biopolymer can be immobilized on the surface due to steric constraints and kinetic factors. Hence, the “grafting-to” method generally results in brushes with small grafting densities and film thicknesses.

The “grafting from” approach (Figure 1.7) has attracted considerable attention in recent years in the preparation of tethered polymers on a solid substrate surface. The initiators are immobilized onto the surface followed by *in situ* surface-initiated polymerization (non-controlled or controlled polymerization) generating linked polymers. The immobilization of initiators on the substrate surface can be achieved with plasma treatment or UV irradiation of the surface.

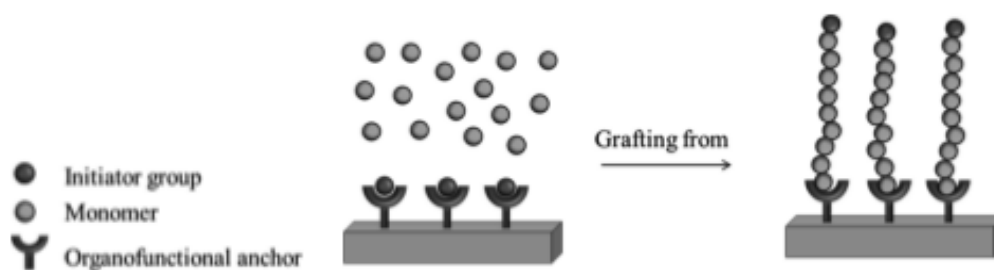


Figure 1.7: "Grafting from" technique

This technique provides a viable alternative to control the functionality, density, and thickness of the polymer brushes [35]. The “grafting from” and “grafting to” techniques can be implemented together. For instance, Berger reported that the first polymer could be immobilized onto one side of silica particles using the “grafting from” approach and the second polymer was grafted onto the other side of the particle surface via the “grafting to” approach.

1.5 The chitosan in biomedical applications

Generally, for improving biocompatibility, biomolecules are natural proteins and polysaccharides. as collagen, fibrin, natural silk, and chitosan.

Among polysaccharides, chitosan with its excellent properties such as biocompatibility, biodegradability and non-toxicity, is typically considered an interesting material for biomedical

application.

Chitosan is a polysaccharide derived from the deacetylation of chitin, one of the most abundant polysaccharides in nature after cellulose, usually obtained from shells of crustaceans, as crab, shrimp, and crawfish [36]. During the process of deacetylation, the water-insoluble chitin (Molecular weight > 1000 kDa) changes to chitosan (Molecular weight > 100 kDa) that is poorly soluble in water [37].

Chemically, chitosan is a polymeric material comprised of N-acetylglucosamine and glucosamine copolymer units. As shown in figure 1.8, the chains of chitosan contain hydroxyl and amine groups, which make it an attractive reactive polymer.

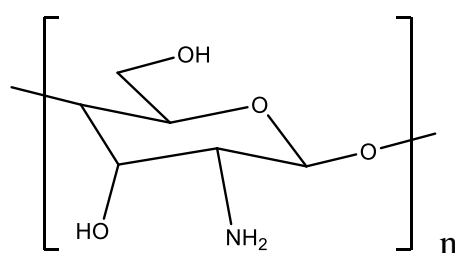


Figure 1.8: Chemical structure of chitosan

The primary uses of chitosan as a substrate include drug and growth factor delivery, and as a scaffold material for particular types of tissue (bone) engineering.

Regarding the material's properties, the characteristics of chitosan are dependent on structural parameters such as molecular weight and its degree of deacetylation. Moreover, the source of extraction and procedures adapted to conduct deacetylation may affect the final properties. The extent of deacetylation strongly influences physical, chemical and biological properties. It is usually available in low medium and high molecular weights and can be used according to the intended application alone or in composite formulations.

Its pH-dependent versatility at a low pH can cause amine groups to be protonated, exhibiting a polycationic nature. At higher pH, chitosan amines are deprotonated and reactive, hence promoting intermolecular interactions advances the formation of fibres, films, porous scaffolds or even gels. Properties such as mechanical strength, biodegradability, and cell affinity can be tailored using various chemical modifications including cross-linking.

Chitosan has been combined with a variety of materials, such as alginate, hyaluronic acid, calcium phosphate, poly(methyl methacrylate) (PMMA), poly(L-lactic acid) (PLLA), and poly-(lactic-co-glycolic acid)-(PGLA) for potential application in orthopaedics and cell-based [38].

Chitosan is osteoconductive, enhancing bone formation both *in vitro* and *in vivo*, but its mechanical weakness and instability, together with its incapacity to maintain a predefined shape, narrows its application field.

Chitosan has been recognised as an antimicrobial agent. However its ability to act in this way is not completely elucidated and several different mechanisms have been reported to this nature of chitosan. One theory suggests that when exposed to bacterial cell wall, chitosan promotes the displacement of Ca^{++} of anionic sites of the membrane, resulting in cellular destruction. Chitosan has a high degree of biocompatibility in animal models and can be conveniently adapted for the development of implantable biomaterials. In addition, chitosan can be chemically functionalized using various compounds.

Due to the chemical structure of chitosan, specific reactions can be performed on the amino group in C-2 position of the glucosamine unit, especially by reductive amination reaction. Also two -OH groups are available on C-3 and C-6 positions. Two different types of derivatives may be recognized: (i) derivatives obtained by chemical modification and introduction of different substituents, (ii) grafted copolymers on C-2 position [39].

Chitlac is a biocompatible modified polysaccharide composed of a chitosan backbone to which lactitol moieties were chemically inserted via a reductive N-alkylation reaction with lactose, as shown in figure 1.9 [40].

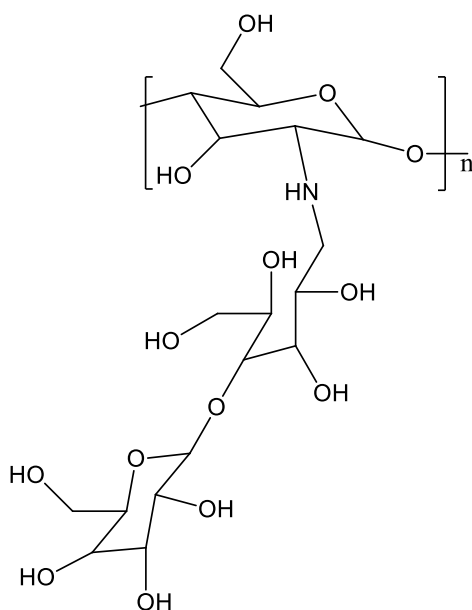


Figure 1.9 Chemical structure of chitlac

The modification of the biopolymer chain with lactose moieties have been firstly investigated by Yalpani et al. in 1985 that established the chemical conditions for the modification of chitosan

[41]. Although chitlac is not a component of the natural extracellular matrix, it represents interesting a natural polymer for the development of biomaterials for tissue regeneration. In particular, it has shown to induce aggregation of articular chondrocytes stimulating the production of collagen and glycosaminoglycans within an otherwise inert 3D architecture. [42,43]. Furthermore, it has also non-biomedical application as wound dressings, cosmetics components, fibres, metal capture materials [44].

1.6 Functionalization of poly(ϵ -caprolactone) for biomedical applications

Poly(ϵ -caprolactone) is a biodegradable biomaterial which does not cause immune responses in human body. Nevertheless, PCL shows poor cell attachment due to its hydrophobicity and inadequate wettability. Surface functionalization is an important strategy to improve the integration of PCL-based biomaterials.

Several strategies have been studied to convert PCL from bioinert PCL into a biologically active polymer [45,46]. PCL surface can be modified by mechanical, physical, chemical or biological methods [47]. The most common used strategy is the changing of surface hydrophobicity [48]. This leads to an activation of polymer surface exhibiting sites for further grafting of biomolecules.

In particular, surface modifications which lead an increased roughness and hydrophilicity promote the immobilization of biomolecules such as proteins and polysaccharides [49].

Desired changes in the PCL backbone can be induced by using energy radiations or wet-chemical methods, as shown schematically in figure 1.10.

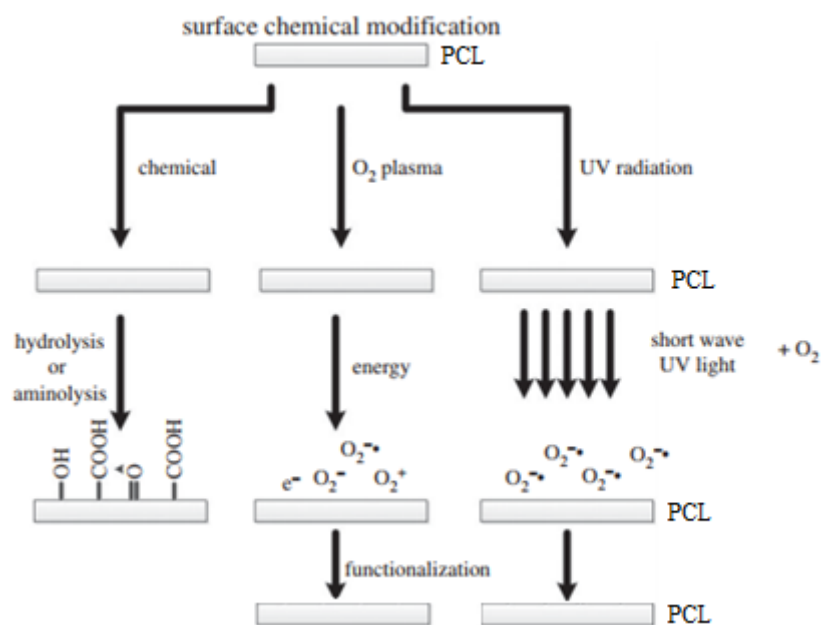


Figure 1.10: Surface chemical modification methods of PCL.

In the radiation-induced grafting, functional groups can be introduced onto the surface of the polymer using different kind of radiation. Ionizing radiation (X-rays, e-beams, γ -rays), mid-energy radiation (laser, plasma sources and UV rays) and low-energy radiation (ultrasonic, microwave and visible sources) exploit the free-radical mechanism to graft the biomolecules [50-51].

In the wet-chemical treatment, the surface PCL activity and roughness can be modified by a chemical reaction of hydrolysis. Functional groups are introduced for a subsequent modification of the surface with biomolecules.

For examples, Sun and coworkers undewent the PCL surface to alkaline hydrolysis treatment to increase the concentration of the carboxyl groups on the surface, for the further for the cell-recognizing peptide grafting [29].

In another study, Xu and coworkers hydrolyzed the PCL, in order to make it react with 2-bromoisobutyryl bromide (BIBB) for the covalent immobilization of atom transfer radical polymerization (ATRP) initiators to produce the PCL-Br surface [52].

Regarding the PCL surface modification by chitosan grafting, only few studies have been reported. In a study by Chen, after introducing carboxyl groups on the surface by oxygen plasma treatment, the PCL nanofibrous membrane (NFM) was covalently grafted with chitosan, using carbodiimide as the coupling agent [53].

Nevertheless, in literature, most of the studies are focused on the blending of PCL and chitosan, for different applications. Wang evaluated the use of a new blend material that can combine the features of chitosan and PCL concurrently. The obtained scaffold is a carrier for growth and differentiation of corneal endothelial cells (CECs) [54]. In another study, Sarasam and coworkers, studied the anti-bacterial properties and changes in physicochemical properties of chitosan upon blending with PCL [55].

An other approach reported by Wang, is the use of copolymerization technique [56]. In this study, for example, an ionic liquid was synthesized and employed as a homogeneous and green reaction media to prepare chitosan-*graft*-polycaprolactone (CS-*g*-PCL) *via* ring-opening polymerization. The chitosan-grafted-PCL copolymer is expected to have the advantageous properties of two polymers and is promising to have some applications in many fields, such as tissue engineering or drug and gene delivery.

In a study of Filova, foam scaffolds from polycaprolactone with incorporated chitosan microparticles were developed to have a potential application in cartilage regeneration [57].

Only in a recent study conducted by Mehr and coworkers, the deposition efficiency of a homogeneous chitosan layer on the surface of a 3D interconnected porous network of PCL, have been proposed [58].

In my study a new approach will be proposed to modify the PCL surface, through the covalent grafting a lactose-modified chitosan (chitlac) on the activated PCL, to improve biocompatibility, for potential application in tissue engineering.

1.7 Functionalization of titanium and its alloys surfaces for biomedical applications

In order to improve the long-term osseointegration of titanium surfaces, various bioactive molecules are grafted in a covalent manner on titanium and its alloys.

For mediating the cellular response, peptides containing the Arg-Gly-Asp (RGD) sequence and signaling proteins such as bone morphogenic proteins (BMPs) have been grafted on the titanium surfaces by a number of groups [30].

In parallel, to minimize bacterial adhesion the covalent bonding of antibacterial moieties to titanium surface, such as the sodium polystyrene sulfonate (poly-NaSS) and the chitosan, was developed.

Indeed, chitosan, is widely investigated for its use as a coating suitable for metallic implants surfaces functionalization for its properties and in particular for its antibacterial characteristics. Indeed, chitosan has a broad spectrum of antimicrobial activities, high bactericidal rates and low toxicity toward mammalian cells, making it a potential biocide also in preserving food [36].

Many approaches have been proposed to attach the chitosan to the metal surface. For example, the layer-by-layer electrostatic deposition of polyelectrolyte multilayers (PEMs), has been used to graft the chitosan on the metal surface. In particular, in a study of 2008, Chua has developed an hyaluronic acid/chitosan PEM-functionalized titanium substrate, immobilized with RGD to enhance mammalian bone cell attachment, proliferation and function, while at the same time conferring antibacterial efficacy [59].

Alternatively, some strategies have been reported to covalently bond chitosan to titanium and Ti6Al4V alloy, using dopamine or organosilane as linker agent.

In detail, in the study by Zao, for example, titanium substrates were surface functionalized with a polydopamine (PDOP) film [60]. Dopamine was employed as an intermediate layer, for post immobilization of chitosan lauric acid conjugate (Chi-LA). The results suggested that Chi-LA conjugate was successfully immobilized onto the surfaces of Ti substrates, with an increasing in terms of cell adhesion, cell viability, intracellular alkaline phosphatase activity and mineralization capacity of osteoblasts when cultured onto Chi-LA surface functionalized Ti substrate.

In a study reported by Hu, the surfaces of titanium substrates were functionalized by covalently grafting of dopamine followed by carboxymethyl chitosan (CMCS) or hyaluronic acid-catechol (HAC) [61]. The CMCS-functionalized titanium demonstrated better antibacterial property than the HAC-functionalized titanium since CMCS is bactericidal.

In other studies reported by Shi, Lim and Ghirime, the titanium and Ti6Al4V alloy were first treated with the dopamine, and then covalently grafted with chitosan, using the glutaraldehyde as coupling agent, with promising results, as shown in figure 1.11. The glutaraldehyde is a common agent for cross-linking or reacting with materials for biomedical application but nevertheless it's toxic [62-64].

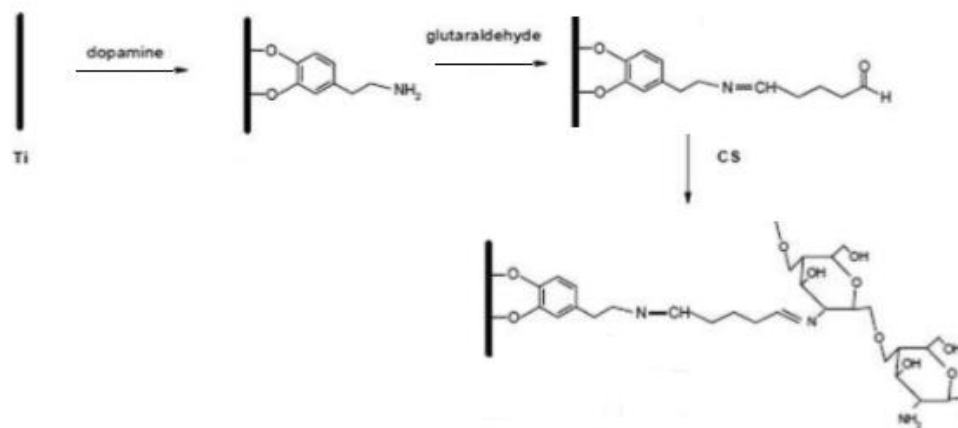


Figure 1.11: The immobilization of Chitosan on Ti substrates by dopamine.

Chitosan can also be immobilized onto metal surface with an organosilane molecule.

3-Aminopropyltriethoxysilane (APTES) is one silane molecule commonly used in the biomedical literature to bond an assortment of materials [65]. Then APTES reacts with a linker molecule, the glutaraldehyde, which will form a covalent bond with the chitosan. Using a silanation, the strength of the bond between chitosan and the metal substrate significantly increases. Indeed, previous studies conducted on chitosan simply deposited on the metal surface presented the formation of weak bond (0.5 MPa).

In another work reported Martin, the chitosan films were bound titanium surface through a three-step process that involved the deposition of 3-aminopropyltriethoxysilane (APTES) in toluene, followed by a reaction between the amine end of APTES with glutaraldehyde, and finally, a reaction between the aldehyde end of glutaraldehyde and chitosan [66]. Two different metal treatments (passivation method and piranha treatment) were examined to determine the ability to bind chitosan. Nevertheless the surface composition of the chitosan films for both of them, were statistically similar, demonstrating that differences in the metal treatments did not affect the chemistry of the chitosan films. In 2008, the same group reported a method, using a silane with one step less. This way involves the grafting of triethoxysilylbutyraldehyde (TESBA) which is directly linked with chitosan [67].

Continuously, new studies about covalent grafting of chitosan on titanium surface have reported in literature in order to find a valid and easy methodology.

In this work of thesis, a new and simple approach of chitosan covalent grafting on titanium and Ti6Al4V surface will be proposed, using a carboxyl group as linker agent.

1.8 References

- [1] F. J. O'Brien. Biomaterials & scaffolds for tissue engineering. *Materials today*, 14(3), 88-95, 2011
- [2] N. R. Patel, P.P. Gohil. A Review on Biomaterials: Scope, Applications & Human Anatomy Significance. *International Journal of Emerging Technology and Advanced Engineering*, 4, 2250-2459, 2012
- [3] G. Heness and B. Ben-Nissan. Innovative Bioceramics. *Materials Forum*, 27, 2004
- [4] E. Gentleman, M. D. Ball, M. M. Stevens. Biomaterials, *Encyclopedia of Life Support Systems*, Medical Sciences, Vol.II, 2016
- [5] S. Seal. Bioceramic Coatings for Medical Implants: Trends and Techniques. *Springer Science & Business Media*, 1, 2010
- [6] C. Auclair-Daigle, M. N. Bureau, J.G. Legoux, & L.H. Yahia. Bioactive hydroxyapatite coatings on polymer composites for orthopedic implants. *Journal of Biomedical Materials Research Part A*, 73(4), 398-408, 2005
- [7] G. Perale, J. Hilborn. Bioresorbable Polymers for Biomedical Applications. 1st Edition, *From Fundamentals to Translational Medicine*, 2016
- [8] M. Askari. Polymer Optic Technology. *Optics*, 4, 1-12, 2015
- [9] S.Kara. A Roadmap of Biomedical Engineers and Milestone. *Biomaterials*, 1st Edition, Intech, 67-114, 2012
- [10] J.Y. Wong, J. D. Bronzino, D. R. Peterson. *Biomaterials: Principles and Practices*. CRC Press, 2012
- [11] G. BaoLin and P.X. MA. Synthetic Biodegradable Functional Polymers for Tissue Engineering: A Brief Review. *Science China Chemistry*, 57(4), 490–500, 2014
- [12] M.A Woodruff and D.W Hutmacher, Dietmar. The return of a forgotten polymer: Polycaprolactone in the 21st century. *Progress in Polymer Science*, 35(10), 1217-1256, 2010
- [13] M. Labet, & W. Thielemans. Synthesis of polycaprolactone: a review. *Chemical Society Reviews*, 38(12), 3484-3504, 2009
- [14] B. D. Ulery, L.S. Nair, & C.T. Laurencin. Biomedical Applications of Biodegradable Polymers. *Journal of Polymer Science. Part B, Polymer Physics*, 49(12), 832–864, 2011

- [15] W. Zheng, D. Guan, Y. Teng, Z. Wang, S. Zhang, L. Wang, & J. Zhang. Functionalization of PCL fibrous membrane with RGD peptide by a naturally occurring condensation reaction. *Chinese science bulletin*, 59(22), 2776-2784, 2014
- [16] S. Chen, A. Qizhi & G Thouas. Metallic implant biomaterials. *Materials Science and Engineering*, 87, 1-57, 2015
- [17] M. T. Dove. Structure and dynamics: an atomic view of materials. *Oxford University Press*, 2003
- [18] V. Migonney, C. Falentin-Daudre. *Biomaterials*. Wiley, 2-6, 2014
- [19] F. C. Campbell. Elements of Metallurgy and Engineering Alloys. *ASM International*, 2008
- [20] H. K. D. H. Bhadeshia, Metallurgy of Titanium and its Alloys, Lectures, University of Cambridge, 2001
- [21] K. C. Dee, D. A. Puleo, R. Bizios. *An Introduction to Tissue-Biomaterial Interactions*. Wiley & Sons, 2003
- [22] M. J. Donachie. *Titanium: A Technical Guide*. 2nd Edition, ASM International, 2000
- [23] D. Vasudevan, P. Balashanmugam and G. Balasubramanian. A Study on Compressive Behaviour of Thermal Cycled Titanium Alloy [Ti-6Al-4V]. *International Journal for Research in Emerging Science and Technology*, 2(7), 2015
- [24] Zia Urahman. Electrochemical & osteoblast adhesion study of engineered TiO₂ nanotubular surfaces on titanium alloys. *Materials Science and Engineering*, C58(1), 160-168, 2016
- [25] Shi, Zhilong. Surface functionalization of titanium with carboxymethyl chitosan and immobilized bone morphogenetic protein-2 for enhanced osseointegration. *Biomacromolecules*, 10(6), 1603-1611 (2009).
- [26] M. D'Almeida, J. Amalric, C. Brunon, B. Grosgeat, and B. Toury. Relevant insight of surface characterization techniques to study covalent grafting of a biopolymer to titanium implant and its acidic resistance. *Applied Surface Science*, 327, 296-306, 2015
- [27] G. Wu, P. Li, H. Feng., X. Zhang, & P. K. Chu. Engineering and functionalization of biomaterials via surface modification. *Journal of Materials Chemistry B*, 3(10), 2024-2042, 2015.
- [28] M. Tallawi, E. Rosellini, N. Barbani, M.G. Cascone, R. Rai, G. Saint-Pierre & A.R. Boccaccini. Strategies for the chemical and biological functionalization of scaffolds for cardiac tissue engineering: a review. *Journal of the Royal Society Interface*, 12(108), 2015

- [29] H. Sun and S. Onneby. Facile polyester surface functionalization via hydrolysis and cell-recognizing peptide attachment. *Polymer International*, 55,1336–1340, 2006
- [30] K. Kyzio, Ł. Kaczmarek and A. Kyzioł. Surface Functionalization of Biomaterials. *Handbook of Composites from Renewable Materials*, 4, 2017
- [31] N. Ghimire, J. Luo, R. Tang, Y. Sun, & Y. Deng. Novel anti-infective activities of chitosan immobilized titanium surface with enhanced osteogenic properties. *Colloids and Surfaces B: Biointerfaces*, 122, 126-13, 2014
- [32] L. Minati, C. Migliaresi, L. Lunelli, G. Viero, M. Dalla Serra & G. Speranza. Plasma assisted surface treatments of biomaterials. *Biophysical Chemistry*, 229, 151-164, 2017
- [33] F. Mastrangelo, G. Fioravanti, R. Quaresima, R. Vinci & E. Gherlone. Self-Assembled Monolayers (SAMs): Which Perspectives in Implant Dentistry?. *Journal of Biomaterials and Nanobiotechnology*, 2, 533-543, 2011
- [34] T. Croll, A. O'Connor, G. Stevens & J. Cooper-White. Controllable surface modification of poly(lactic-coglycolic acid) (PLGA) by hydrolysis or aminolysis: I. Physical, chemical, and theoretical aspects. *Biomacromolecules*, 5, 463– 473, 2004
- [35] T. Zhou, Y. Zhu, X. Li, X. Liu, K.W. Yeung, S. Wu, P.K. Chu. Surface functionalization of biomaterials by radical polymerization. *Progress in Materials Science*, 83, 191-235, 2016
- [36] Y. Li, X.G. Chen, N. Liu, C.S. Liu, C.G. Liu, X.H. Meng, & J.F. Kenedy. Physicochemical characterization and antibacterial property of chitosan acetates. *Carbohydrate polymers*, 67(2), 227-232, 2007
- [37] Husain, Shehriar. Chitosan Biomaterials for Current and Potential Dental Applications. Ed. Jiujiang Yu, *Materials*, 10(6), 602, 2017
- [38] Venkatesan, Jayachandran, and K. Se-Kwon. Chitosan Composites for Bone Tissue Engineering-An Overview. *Marine Drugs*, 8(8), 2252–2266, 2010
- [39] P. Le Dung, M. Milas, M. Rinaudo, & J. Desbrières. Water soluble derivatives obtained by controlled chemical modifications of chitosan. *Carbohydrate Polymers*, 24(3), 209-214, 1994
- [40] P. Marcon, E. Marsich, A. Vetere, P. Mozetic, C. Campa I. Donati & S. Paoletti. The role of Galectin-1 in the interaction between chondrocytes and a lactose-modified chitosan. *Biomaterials*, 26(24), 4975-4984, 2005

- [41] M. Yalpani, L. D. Hall, M. A. Tung Yalpani, M., Hall, L. D., Tung, M. A., & D.E. Brooks. Unusual rheology of a branched, water-soluble chitosan derivative. *Nature*, 302(5911), 812-814, 1983
- [42] M.Cok, P. Sacco, D. Porrelli, A. Travan, M. Borgogna, E. Marsich, S. Paoletti & I. Donati. Mimicking mechanical response of natural tissues. Strain hardening induced by transient reticulation in lactose-modified chitosan (chitlac). *International Journal of Biological Macromolecules*, 2017
- [43] E. Marsich, M. Borgogna, I. Donati, P. Mozetic, B.L. Strand, S.Salvador, F.Vittur & S.Paoletti. Alginate/lactose-modified chitosan hydrogels: a bioactive biomaterial for chondrocyte encapsulation. *Journal of biomedical materials research A*, 84, 364-376, 2008
- [44] M. Kozicki, M. Kołodziejczyk, M. Szyrkowska, Al. Pawlaczyk, E. Leśniewska, A. Matusiak, A.Adamus & A. Karolczak. Hydrogels made from chitosan and silver nitrate. *Carbohydrate Polymers* 140, 74-87, 2016
- [45] H. A. Declercq, T. Desmet, E.E. Berneel, P. Dubruel, & M.J. Cornelissen. Synergistic effect of surface modification and scaffold design of bioploted 3-D poly-ε-caprolactone scaffolds in osteogenic tissue engineering. *Acta biomaterialia*, 9(8), 7699-7708, 2013
- [46] S.M. Giannitelli, F.Abruzzese, P. Mozetic, A. De Ninno, L.Businaro, L., Gerardino, & A. Rainer. Surface decoration of electrospun scaffolds by microcontact printing. *Asia-Pacific Journal of Chemical Engineering*, 9(3), 401-406, 2014
- [47] E.D. Yildirim, D. Pappas, S. Güçeri & W. Sun. Enhanced cellular functions on polycaprolactone tissue scaffolds by O₂ plasma surface modification. *Plasma Processes and Polymers*, 8(3), 256-267, 2011
- [48] A.S. Hoffman. Surface modification of polymers: physical, chemical, mechanical and biological methods. *Macromolecular Symposia*, 1996
- [49] M. Takeuchi. Acid pretreatment of titanium implants. *Biomaterials*, 24(10), 1821-1827, 2000
- [50] D. Ribuffo, F. Lo Torto, S. M. Giannitelli, M. Urbini, L. Tortora, P. Mozetic, M. Trombetta, F. Basoli, S. Licoccia, V. Tombolini, R. Cassese, N. Scuderi & A. Rainer. The effect of post-mastectomy radiation therapy on breast implants: Unveiling biomaterial alterations with potential implications on capsular contracture. *Material Science and Engineering* 57, 338-343, 2015
- [51] T. Desmet, R. Morent, N.D. Geyter, C.Leys, E. Schacht & P. Dubruel. Nonthermal plasma technology as a versatile strategy for polymeric biomaterials surface modification: a review. *Biomacromolecules*, 10(9), 2351-2378, 2009

- [52] F. J. Xu, Z. H. Wang, & Yang. Surface functionalization of polycaprolactone films via surface-initiated atom transfer radical polymerization for covalently coupling cell-adhesive biomolecules. *Biomaterials*, 31(12), 3139-3147, 2010
- [53] S.H. Chen, C.H. Chen, Y.T. Fong, Y. T., & J.P. Chen. Prevention of peritendinous adhesions with electrospun chitosan-grafted polycaprolactone nanofibrous membranes. *Acta biomaterialia*, 10(12), 4971-4982, 2014
- [54] T. J. Wang, J.N. Lu & T. H. Young. Novel chitosan-polycaprolactone blends as potential scaffold and carrier for corneal endothelial transplantation. *Molecular vision*, 18, 255, 2012
- [55] A.R. Sarasam, R.K. Krishnaswamy & S.V. Madihally. Blending chitosan with polycaprolactone: effects on physicochemical and antibacterial properties. *Biomacromolecules*, 7(4), 1131-1138, 2006
- [56] Z. Wang, L. Zheng, C. Li, D. Zhang, Y. Xiao, G. Guan, & W. Zhu. A novel and simple procedure to synthesize chitosan-graft-polycaprolactone in an ionic liquid. *Carbohydrate polymers*, 94(1), 505-510, 2013
- [57] E. Filová, B. Jakubcová, I. Danilová, E. Kuželová Košťáková, T. Jarošíková, O. Chernyavskiy, J. Hejda, M. Handl, J. Beznoska, A. Nečas, J. Rosina, E. Amler. Polycaprolactone Foam Functionalized With Chitosan Microparticles - A Suitable Scaffold For Cartilage Regeneration. *Physiological research*, 65, 121-131, 2016
- [58] N. G. Mehr, C.D. Hoemann, & B.D Favis. Chitosan surface modification of fully interconnected 3D porous poly (ϵ -caprolactone) by the LbL approach. *Polymer*, 64, 112-121, 2015
- [59] P.H. Chua, K.G. Neoh, E.T. Kang, & W. Wang. Surface functionalization of titanium with hyaluronic acid/chitosan polyelectrolyte multilayers and RGD for promoting osteoblast functions and inhibiting bacterial adhesion. *Biomaterials*, 29(10), 1412-1421, 2008
- [60] L. Zhao, L., Y. Hu, D. Xu, & K. Cai. Surface functionalization of titanium substrates with chitosan-lauric acid conjugate to enhance osteoblasts functions and inhibit bacteria adhesion. *Colloids and Surfaces B: Biointerfaces*, 119, 115-125, 2014
- [61] X. Hu, K. G. Neoh, Z. Shi, E. T. Kang, C. Poh, & W. Wang. An in vitro assessment of titanium functionalized with polysaccharides conjugated with vascular endothelial growth factor for enhanced osseointegration and inhibition of bacterial adhesion. *Biomaterials*, 31(34), 8854-8863, 2013

- [62] Z. Shi, K.G Neoh, E.T. Kang, C. Poh & W. Wang. Bacterial adhesion and osteoblast function on titanium with surface-grafted chitosan and immobilized RGD peptide. *Journal of Biomedical Materials Research Part A*, 86(4), 865-872, 2008
- [63] T.Y Lim, W. Wang, Z. Shi, C.K. Poh, K.G. Neoh. Human bone marrow-derived mesenchymal stem cells and osteoblast differentiation on titanium with surface-grafted chitosan and immobilized bone morphogenetic protein-2. *Journal of Materials Science: Materials in Medicine*, 20(1), 2009
- [64] N. Ghimire, J. Luo, R. Tang, Y. Sun, & Y. Deng. Novel anti-infective activities of chitosan immobilized titanium surface with enhanced osteogenic properties. *Colloids and Surfaces B: Biointerfaces*, 122, 126-133, 2014
- [65] A. Nanci, J.D. Wuest, L. Peru, P. Brunet, V. Sharma, S. Zalzal, & M.D. McKee. Chemical modification of titanium surfaces for covalent attachment of biological molecules. *Journal of Biomedical Materials Research A*, 40(2), 324-335, 1998
- [66] H. J. Martin, K. H. Schulz, J. D., Bumgardner, & K. B. Walters. XPS study on the use of 3-aminopropyltriethoxysilane to bond chitosan to a titanium surface. *Langmuir*, 23(12), 6645-6651, 2007
- [67] H.J. Martin, K.H. Schulz, J.D. Bumgardner, J.A. Schneider. Enhanced bonding of chitosan to implant quality titanium via four treatment combinations. *Thin Solid Films*, 516 (18): 6277–6286, 2008

Chapter 2

Aim of the thesis

Aim of this thesis was to develop new strategies of biomaterials functionalization, both polymeric and metal biomaterials, in order to minimize bacterial adhesion and improve the interaction between materials and tissues.

Chapter 3 deals with the functionalization and subsequent characterization of poly(ϵ -caprolactone) (PCL) with lactose-modified chitosan (chitlac) grafting, using as activation treatment of the substrate, the alkaline hydrolysis. Each step of functionalization will be characterized by Time of Flight Secondary Ion Mass Spectrometry (ToF-SIMS), a very sensitive technique, which provides detailed elemental and molecular information about the surface, thin layers, interfaces of the sample, and gives a full three-dimensional analysis, with high mass resolution and high lateral resolution. In detail, obtained results will be compared to ones, relative to the chitlac only physisorbed on the pure PCL, analyzing statistically ToF-SIMS data, by Principal Component Analysis (PCA). Furthermore, the functionalization efficiency of chitlac with two different derivatization degrees (64 % and 9%) will be evaluated, to identify which is the chitlac that adheres more on the surface.

In the chapter 4, both titanium and Ti6Al4V alloy will be functionalized with chitosan. Different pretreatments of metal surface, in particular the etching treatments, will be test to evaluate the one which permits the best chitosan functionalization. The grafting will be obtained with a very easy process, because the chitosan will be attached to the surface, activated by simple carboxylation procedure. Each step of grafting will be analyzed by Fourier Transform IR (FTIR) and X-ray Photoelectron Spectroscopy (XPS) techniques for a complete characterization, both qualitative and quantitative. Furthermore, also an electrochemical method, the cyclic voltammetry, will be used to assess qualitatively the presence of the chitosan on the surfaces, obtained after grafting process.

The objective of this research is to provide some valid methodologies of biomaterial surface functionalization, in order to meet future demands on orthopedic devices and tissue engineering, particularly in the context of enhancing osseointegration and removing the infectious complications, after implantation.

Chapter 3

Functionalization of poly(ϵ -caprolactone) surface with lactose-modified chitosan via alkaline hydrolysis

In this study, a novel functionalization of poly(ϵ -caprolactone) (PCL) was performed via hydrolysis and subsequent lactose-modified chitosan (chitlac) attachment.

In the first step of functionalization, the PCL film, which was previously prepared using the casting technique, was activated by alkaline hydrolysis treatment, for exhibiting initiating sites for the further grafting of biomolecule. This treatment increased the concentration of carboxyl groups on the PCL surface and it enhanced the roughness substrate, a factor that affect cellular response to the biomaterial [1].

In the second step, chitlac A and chitlac B, the lactose modified chitosan variants with two different degree of derivatization (respectively 64% and 9%) were synthesized dissolving the chitosan in a mixture of methanol and acetic acid followed by the addition of the same solvent mixture containing lactose and sodium cyanoborohydride (figure 3.1).

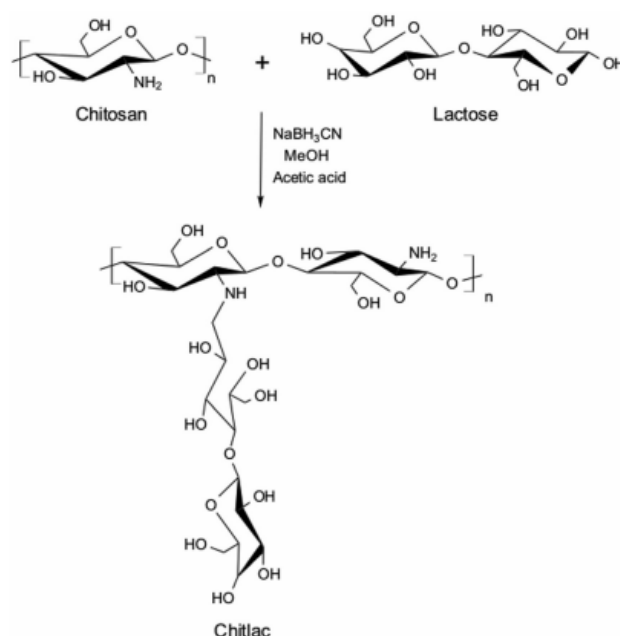


Figure 3.1: Synthesis of chitlac via N-alkylation of chitosan with lactose.

Later, the chitlac (A or B) was grafted to the activated PCL surface, with formation of amide bonds between hydrolyzed PCL substrate carboxyl groups and amine residues of chitlac. The activation of the reaction, necessary for the formation of the peptide bond, was introduced by the 1-ethyl-3-(3-dimethylaminopropyl) carbodiimide hydrochloride (EDC) coupling agent. The EDC efficiency was

improved, also adding N-hydroxysuccinimide (NHS) in the 2-(N-morpholino)ethanesulfonic acid sodium salt) buffer solution (MES).

Each step of functionalization was characterized by the Time of flight secondary ion mass spectrometry (ToF-SIMS), in synergy with univariate and multivariate statistical analysis (Principal Component Analysis). The obtained results were compared to the control sample ones, where the chitlacA/B will be only physisorbed on the blank PCL surface, permitting also to discriminate the two different chitlac variants.

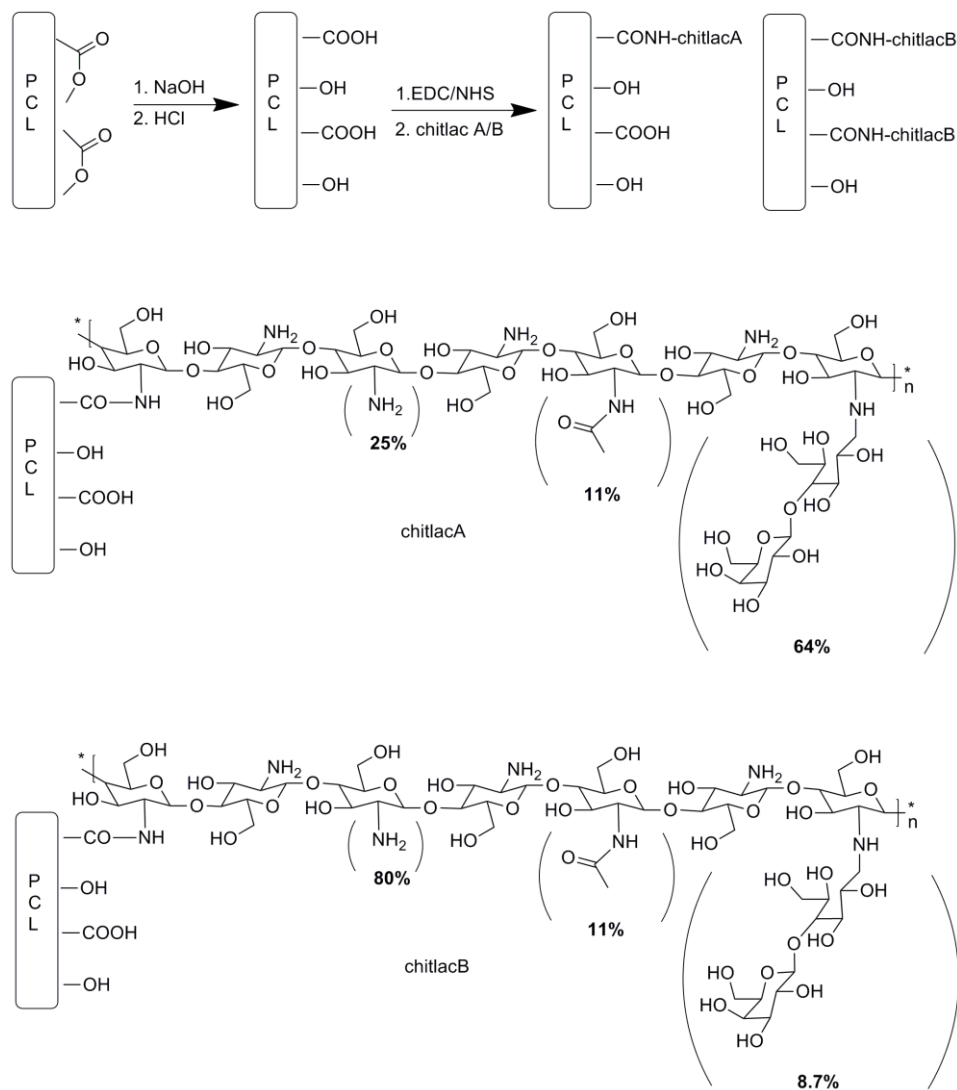


Figure 3.2: Surface carboxylation of PCL and immobilization of chitlac A and B.

3.1. MATERIALS

Chitosan with a medium molecular weight of 250 kDa and a deacetylation degree of 75-85%, PCL with a molecular weight of 80 kDa, were purchased from Sigma Aldrich (Milwaukee, WI). Also the 1-ethyl-3-(3-dimethylaminopropyl) carbodiimide hydrochloride (EDC), the N-hydroxysuccinimide (NHS) and the 2-(N-morpholino)ethanesulfonic acid (MES, 0.1M, pH=6.20) buffer, used for the biomolecule grafting, were purchased from Sigma.

3.1.1 Synthesis of lactosylated chitosan (*chitlac*)

Lactose-modified chitosan, *chitlac*, was synthesized according to previous authors [2]. Briefly, two different N-alkyl derivatives (*chitlacA* and *chitlacB*) of purified chitosan were synthesized by dissolving 1g of chitosan in a 70 mL of a 1:1 mixture of methanol and 1% acetic acid (pH 4.5) followed by the addition of 20 ml of the same solvent mixture containing lactose and sodium cyanoborohydride (amount of reagents is reported in Table 3.1) under mild stirring. The reaction was performed for 24 hours at RT. After dilution with deionized water, the solution was exhaustively dialyzed against deionized water and lyophilized.

Sample	Lactose (g)	NaBH ₃ CN (g)	Composition GlcNH-Lac (%)
<i>chitlacA</i>	4.1	1.82	64.3
<i>chitlacB</i>	1.31	0.909	8.7

Table 3.1: Amount of reagents used in the synthesis of *chitlacA* and *B*. % lactosilation: Degree of N-alkylation of chitosan with lactose.

3.1.2 Preparation of PCL films by casting technique

Poly(ϵ -caprolactone) films were prepared dissolving 8% w/v PCL in 70:30 v/v dichloromethane/methanol mixture. The solution was uniformly cast on a glass plate by means of doctor blade equipment (gap set at 150 μ m) and dried at room temperature.

After complete evaporation of the solvent, substrates were activated by slightly modifying a previously developed protocol [3] as described in detail in the following paragraphs.

3.1.3 Base-catalyzed hydrolysis treatment of the PCL film surface

PCL films underwent controlled surface hydrolysis by incubation in 0.1 M NaOH at 37° C for 90 min, followed by protonation in 0.01 M HCl for 30 min at RT, leading to an increase in carboxyl groups on the PCL surface. Experiments were performed in triplicate.

3.1.4 Immobilization of chitlacA and chitlacB on the PCL film

Activated PCL films were immersed in a catalyst solution containing 0.4M EDC and 0.1M NHS, in MES buffer (0.1M, pH=6.20). After reaction for 1 hour in this mixture, samples were rinsed in MES and then reacted with a 1% w/v chitlac in MES solution for 1 hour at RT. Covalent coupling was obtained through the reaction between carboxyl groups of the activated PCL substrate and free amino groups of chitlac, according to the reaction scheme reported in Figure 3.1. Finally, samples were exhaustively washed with deionized water in order to remove non-grafted molecules.

Non-activated membranes were used as a control in order to study the plain adsorption of chitlac on PCL surface. Table 3.2 reports samples nomenclature as a function of process conditions.

Sample name	Treatment	
	Hydrolysis	Grafting
PCLctrl	-----	-----
PCLhydro	NaOH 90 min, HCl 30 min	-----
PCLActrl	-----	chitlacA
PCLBctrl		chitlacB
PCLAhydro	NaOH 90 min, HCl 30 min	EDC/NHS + chitlacA
PCLBhydro		EDC/NHS + chitlacB

Table 3.2: Samples nomenclature and process conditions.

3.2 METHODS

3.2.1 Scanning electron microscopy (SEM) characterization

Morphological analysis of PCL membranes was studied by field-emission gun scanning electron microscopy (FEG-SEM, Leo 35, Carl Zeiss, Germany). Samples were mounted on metal stubs and gold sputtered (K550x, Emitech, UK) and observed at an accelerating voltage of 5 kV.

3.2.2 ToF-SIMS characterization

PCL, chitosan, chitlacA and chitlacB were analyzed as pure matter to obtain the reference spectra. PCL films were studied before and after hydrolysis treatment. Thin films of chitosan, chitlacA and chitlacB were prepared for ToF-SIMS analysis by casting polymer solutions onto silicon substrates. ToF-SIMS measurements were performed with a ToF-SIMS 5 (ION-TOF GmbH, Germany) spectrometer, using a cluster of Bi_3^+ primary ion source. The cycle time was set to 160 μs , in order to obtain a positive and negative ion ToF-SIMS spectra with a mass range from 1 to 1000 m/z. Samples were probed with a pulsed primary beam (~ 0.3 pA), operated at 30 keV, aimed to ensure the primary “ion dose” remains below the static SIMS limits (10^{12} ions/cm²). Spectra were acquired in high current bunched mode (i.e. high-mass resolution mode) with a mass resolution at m/z 69 (C_5H_9^+) of about 5000 m/ Δ m. A pulsed low energy electron flood gun ($E_k=20$ eV) was used to minimize charging effects due to the isolating properties of samples. The scanning area of secondary ions was 200 $\mu\text{m} \times 200 \mu\text{m}$ with a resolution of 128 pixel \times 128 pixel for all the measurements. Secondary ion images were normalized dividing the mass spectra at each pixel by the total ion image at that pixel. This step was indispensable to reduce topographic effect due to the non-smooth surface of samples.

Raw data were acquired, calibrated, analyzed and exported for further analysis by SurfaceLab 6.4v software. Standard deviations were calculated from measurements performed on three different area.

Spectra calibration was achieved using positions of C^+ , CH^+ , CH_2^+ , CH_3^+ , C_2H_3^+ , peaks in positive mode and C^- , CH^- , CH_2^- , C_2^- and C_2H^- peaks in negative mode.

3.2.3 Statistical data analysis

Univariate analysis, was performed using Origin ver. 9.1 (OriginLab, Northampton, MA). As with many statistical methods, it is recommended to preprocess the raw data, to highlight the true chemical differences in the samples. The foremost preprocessing of ToF-SIMS data is the normalization in order to remove the differences due to sample charging and instrument variations during the analysis. ToF-SIMS spectra were normalized to the sum of the selected peaks, to prevent the influence of contaminants.

Conditions of normality (i.e., data following a normal distribution) were checked using Shapiro-Wilk test. Analysis of variance was used to compare the relative fragment ion signal intensities among different groups, followed by posthoc multiple pairwise comparisons (Tukey test). Values were considered as significant when the p-value was below the 5% confidence level ($p < 0.05$). Data are presented as mean \pm standard deviation.

Multivariate analysis (PCA) was performed using a purposely developed script in MATLAB 2013a (the MathWorks, Inc., Natick, MA). PCA is a powerful tool used to find combinations of variables that describe trends in large amounts of data. PCA was combined with ToF-SIMS data to extract information and relations between chemical species (loadings) and samples (scores).

Before PCA, the data set was also mean-centered. Mean centering centers the data so that all the variables vary across a common mean of zero, providing differences in the relative intensities and not in the means of variables. PCA data were presented using score and loading plots. Each observation displayed in the scores plots was obtained from an average of three representative mass spectra recorded for each experiment. Averages of mass spectra were needed to avoid topography effects due to the irregular surface of PCL.

3.3 RESULTS AND DISCUSSIONS

3.3.1 SEM characterization

Morphological analysis was performed to evaluate possible modifications related to the functionalization treatment. Since no evident differences were detected between the two chitlac-functionalized samples during the analysis, only chitlacA was considered for representative purposes. Figure 3.3 shows SEM micrographs of untreated and functionalized substrates after physi- and chemisorption processes.

As already stated by previous authors [4], the surface of PCL film obtained by solution casting showed the presence of spherulitic structures immersed inside an amorphous matrix (Figure 3.3 A,

B). After chemical functionalization (Figures. 3.3 E,F), the surface of PCL films (PCLAhydro) showed topographical modifications reliably induced by hydrolysis treatment [5], while PCL substrate following physisorption (PCLActrl, Figures. 3.3 C,D) maintained high similarity with untreated substrate (PCLctrl, Figs. 3.3 A,B).

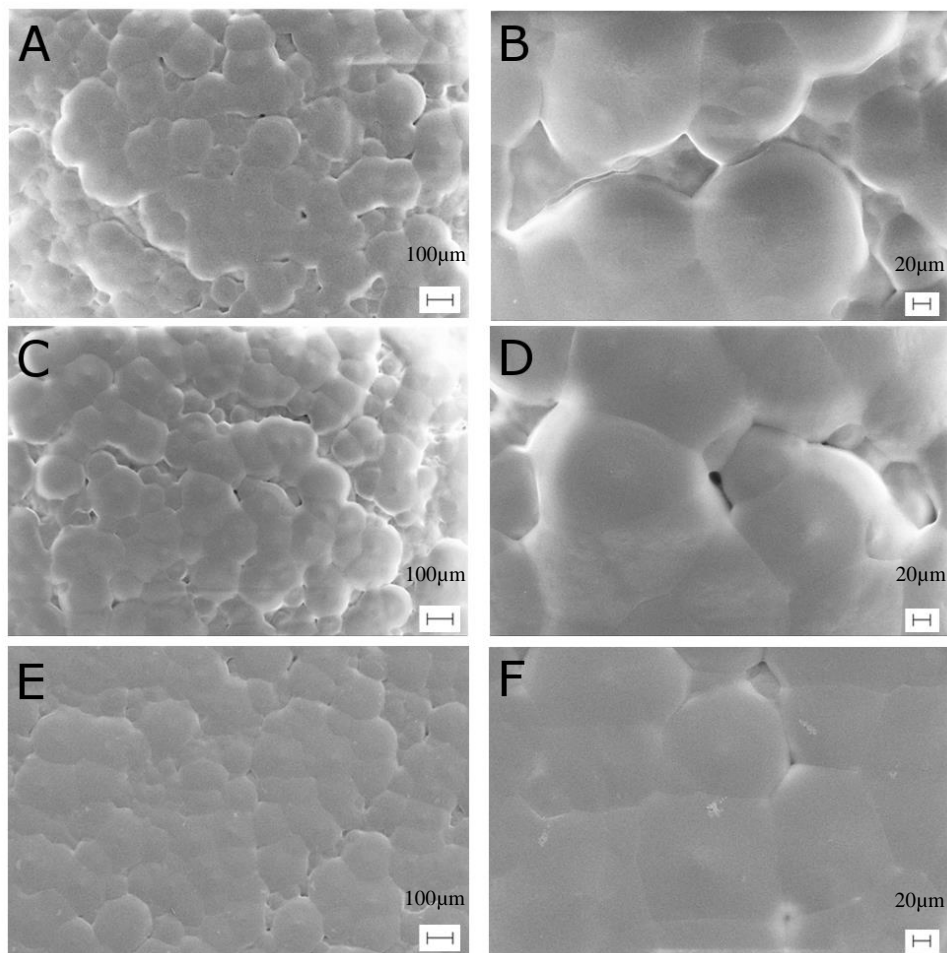


Figure 3.3 SEM micrographs of PCLctrl (A,B), PCLActrl (C,D) and PCLAhydro (D,E) at different magnifications. Scale bars: 100 μm (A,C and E) and 20 μm (B,D,F).

3.3.2 ToF-SIMS reference spectra from PCL membrane, chitosan and chitlac

As first step of our study, ToF-SIMS reference spectra of blank poly(ϵ -caprolactone), chitosan and chitlac were acquired. For the pure poly(ϵ -caprolactone), all the most intense peaks reported in literature [6-8] were also found in control PCL (PCLctrl), both in positive and negative ion mode. After alkaline hydrolysis of PCL film, the mass spectrum of the PCL membrane (PCLhydro) in positive ion mode was dominated by hydrocarbon and sodium peaks, as shown in figure 3.4a.

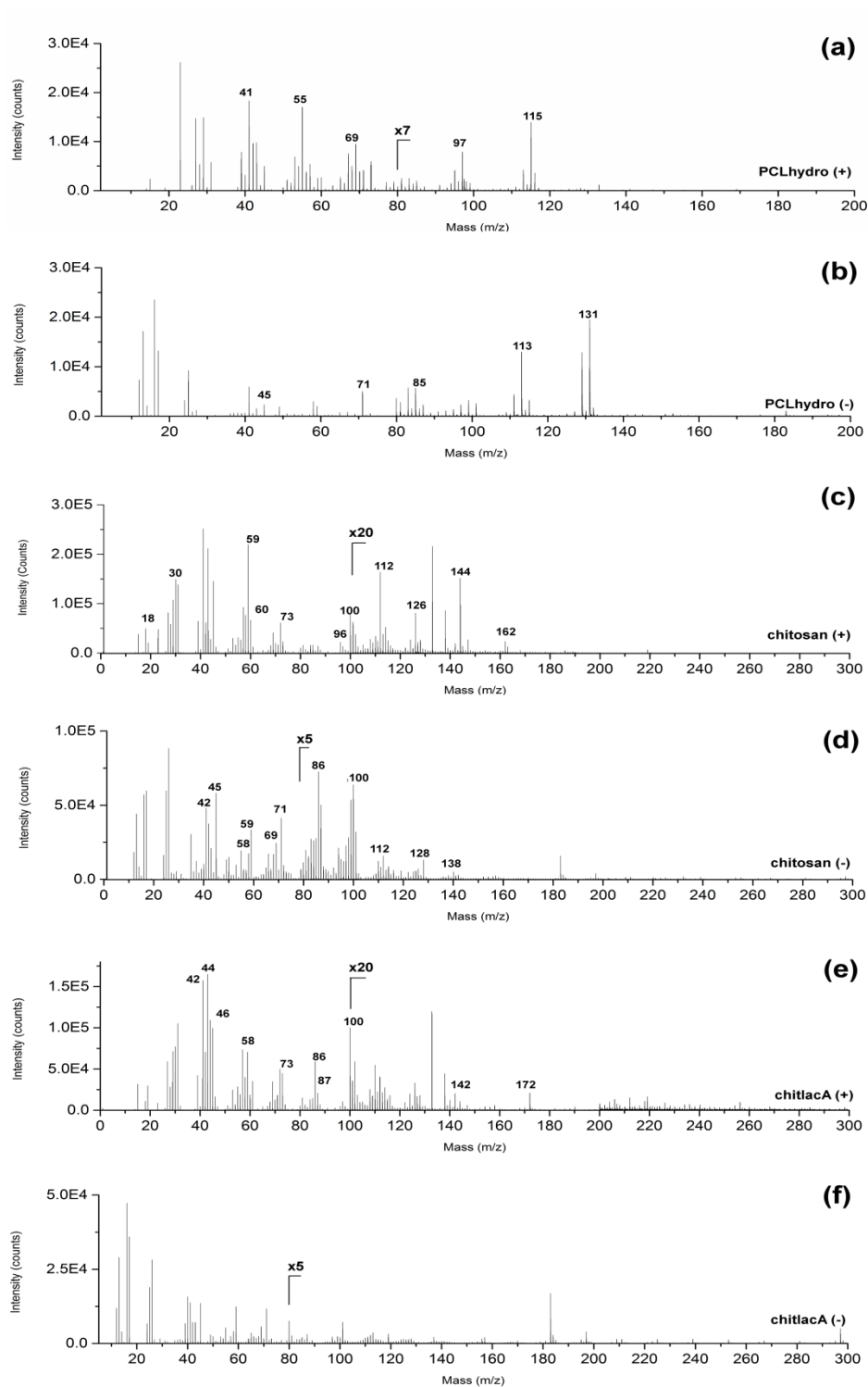


Figure 3.4: Partial positive and negative ToF-SIMS spectra of standard samples. (a,b) hydrolyzed PCL with m/z from 1 to 200, (c,d) chitosan standard with m/z from 1 to 300 and (e,f) ChitlacA standard with m/z from 1 to 300.

In detail, peaks at m/z 41($C_3H_5^+$), 55($C_3H_3O^+$), 69($C_5H_9^+$), 97($C_6H_9O^+$) and the protonated monomer 115($C_6H_{11}O_2^+$), were observed in positive polarity. The negative mass spectrum, showed in figure 3.4b, contained peaks at m/z 45($COOH^-$), 71($C_3H_3O_2^-$), 85($C_5H_9O^-$), 113($C_6H_9O_2^-$), 131($C_6H_{11}O_3^-$). No peaks attributable to nitrogen-containing fragments were revealed.

Chitosan was analyzed as pure substance. In this case, several new peaks were detected, both in positive and negative polarity, that could be assigned to nitrogen containing fragments. Some of these assignments were already found in literature [9-10]. In figure 3.4c, positive mass spectrum of chitosan are reported. Molecular fragments at m/z 18(NH_4^+), 30(CH_4N^+), 59($\text{C}_3\text{H}_7\text{O}^+$), 60($\text{C}_2\text{H}_6\text{NO}^+$), 73($\text{C}_3\text{H}_7\text{NO}^+$), 96($\text{C}_5\text{H}_6\text{NO}^+$), 100($\text{C}_4\text{H}_6\text{NO}_2^+$), 112($\text{C}_5\text{H}_6\text{NO}_2^+$), 144($\text{C}_6\text{H}_{10}\text{NO}_3^+$) were found. In addition, peaks at m/z 58($\text{C}_2\text{H}_4\text{NO}^+$), 72($\text{C}_3\text{H}_6\text{NO}^+$), 126($\text{C}_6\text{H}_8\text{NO}_2^+$), and the monomer at m/z 162($\text{C}_6\text{H}_{12}\text{NO}_4^+$) were detected.

Negative mass spectrum, reported in figure 3.4d, shows secondary ions at m/z 42(CNO^-), 45(COOH^-), 58($\text{C}_2\text{H}_4\text{NO}^-$), 59($\text{C}_2\text{H}_3\text{O}_2^-$), 71($\text{C}_3\text{H}_3\text{O}_2^-$), 86($\text{C}_3\text{H}_4\text{NO}_2^-$), 100($\text{C}_4\text{H}_6\text{NO}_2^-$). Furthermore, peaks at m/z 43($\text{C}_2\text{H}_3\text{O}^-$), 55($\text{C}_3\text{H}_3\text{O}^-$), 68($\text{C}_3\text{H}_2\text{NO}^-$), 69(C_3HO_2^-), 99($\text{C}_4\text{H}_3\text{O}_3^-$), 112($\text{C}_5\text{H}_6\text{NO}_2^-$), 128($\text{C}_5\text{H}_6\text{NO}_3^-$) and 138($\text{C}_6\text{H}_6\text{NO}_3^-$) were detected.

With regard to the characterization of chitlacA and B, reference mass spectra in both positive (figure 3.4e) and negative (figure 3.4f) ion mode revealed a large number of peaks in common with the chitosan. In spite of this, characteristic peaks were identified in positive polarity at m/z 42($\text{C}_2\text{H}_4\text{N}^+$), 44($\text{C}_2\text{H}_6\text{N}^+$), 46($\text{C}_2\text{H}_8\text{N}^+$), 58 ($\text{C}_3\text{H}_8\text{N}^+$), 73 ($\text{C}_3\text{H}_5\text{O}_2^+$), 86 ($\text{C}_4\text{H}_8\text{NO}^+$), 87 ($\text{C}_4\text{H}_9\text{NO}^+$), 88 ($\text{C}_4\text{H}_{10}\text{NO}^+$), 100 ($\text{C}_5\text{H}_{10}\text{NO}^+$), 142 ($\text{C}_7\text{H}_{12}\text{NO}_2^+$) and 172 ($\text{C}_9\text{H}_{16}\text{O}_3^+$), as showed in figure 3.4e.

3.3.3 Effects of hydrolysis treatment on PCL membrane

In order to evaluate the success of hydrolysis treatment by ToF-SIMS technique, COOH^- signal was studied. The presence of carboxyl groups on PCL surface was fundamental for the subsequent bond with chitlac amino group. Thus, this signal was used as an indicator to confirm and qualitatively evaluate the effects of hydrolysis in terms of surface carboxylation of PCL. Figure 3.5 reports the average normalized intensity of COOH^- fragment in PCLctrl and PCLhydro, respectively. The difference between two signals was statistically significant ($p=0.0216$). Indeed, as we noticed, the signal intensity was greater in hydrolyzed PCL sample than the control one, confirming the success of hydrolysis treatment in increasing the surface carboxyl concentration for the further chitlac attachment.

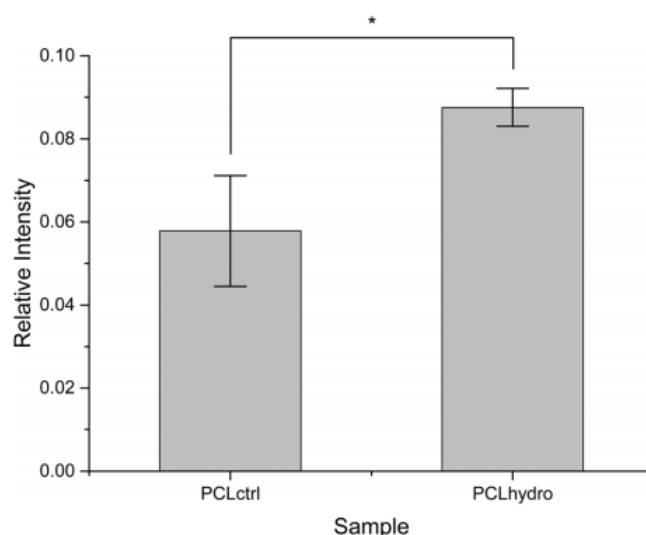


Figure 3.5: Average ionic abundance of COOH fragment in PCLctrl and PCLhydro. Asterisk denotes significance.

3.3.4 Evaluation of the degree of derivatization of chitlac

To confirm the greater degree of derivatization of chitlacA (64%) as compared to chitlacB (8.7%), the mean relative ionic abundance of OH⁻ fragment was evaluated in the reference samples of chitosan, chitlacA and chitlacB samples. In fact, eight hydroxyl groups are contained in the lactose molecule. These additional hydroxyl groups introduced by lactosilation should contribute to increasing the total number of counts recorded for OH⁻ ion in the mass spectrum of chitlacA and chitlacB. As shown in Figure 3.6, the abundance of the OH⁻ group in chitlacA was greater than in chitosan and chitlacB, as expected by the higher degree of chitosan N-alkylation with lactose (Table 3.1). The difference between three signals was statistically significant with p=0.000619.

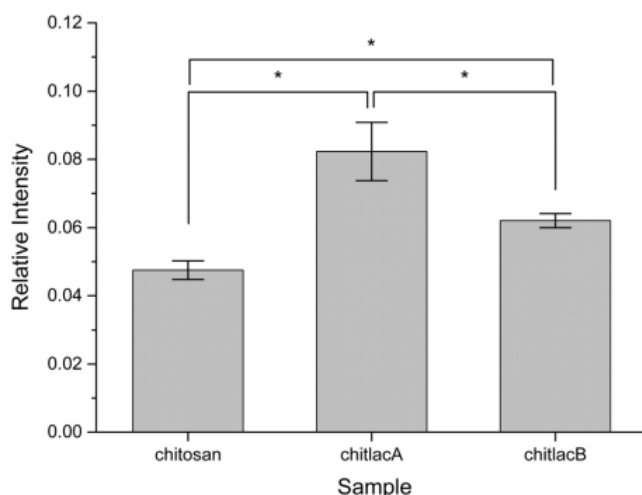


Figure 3.6: Average relative ionic abundance of OH⁻ fragment in chitosan, chitlacA, and chitlacB standards. Asterisk denotes significance.

3.3.5 ToF-SIMS characterization of the chitlac grafting on PCL

Figure 3.7 shows positive ion ToF-SIMS images from PCLAhydro. The homogeneity of chitlac coating on hydrolyzed PCL membrane could be easily verified by the signal distribution of CH_4N and $\text{C}_3\text{H}_8\text{N}$, fragment ions, characteristic respectively of chitosan (fig. 3.7c) and chitlac (fig. 3.7d). Although these images suggested a relatively uniform distribution for chitlac throughout the field of view, by comparing the signal distribution for chitlac with the PCL (fig. 3.7b), it was possible to appreciate small regions of the functionalized membrane where the signals of PCL and sodium (fig. 3.7d) were more intense. On the contrary, in correspondence of the same regions the chitlac image showed a slightly reduced signal. This was an expected result since the hydrolyzed PCL membranes could show regions with irregular surface where the immobilization of chitlac would result more difficult.

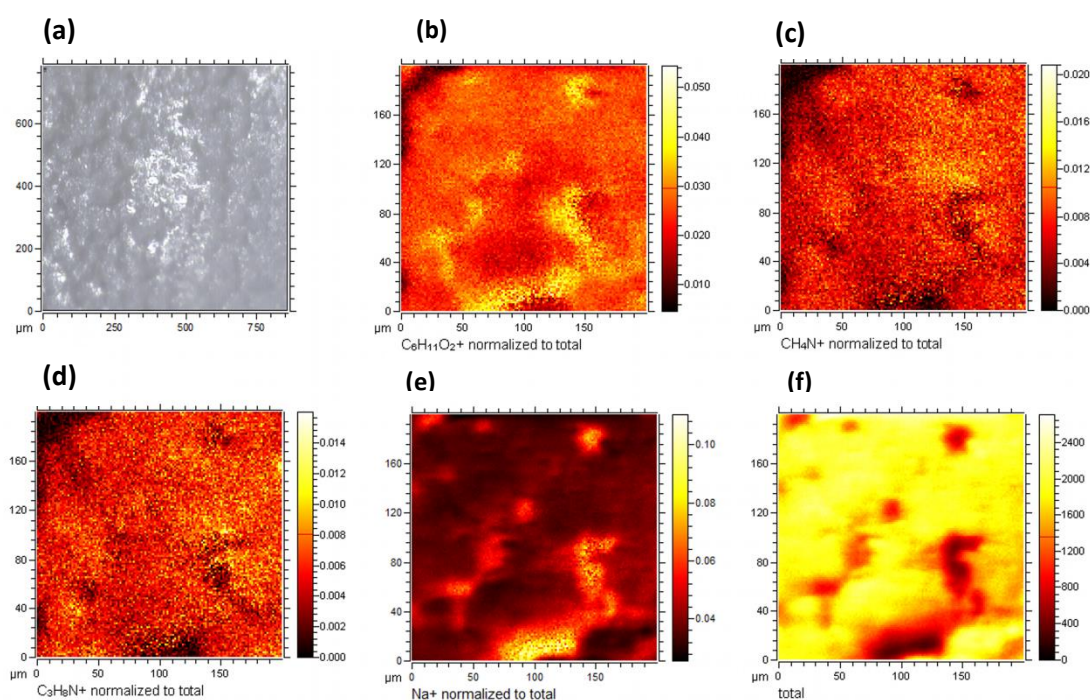


Figure 3.7: (a) Optical image of functionalized PCL membrane. (b-e) Positive-ion ToF-SIMS images of hydrolyzed PCL with chitlacA (PCLAhydro), representing the signal intensity distribution of (b) protonated monomer of PCL (115 m/z), (c) nitrogen containing fragments from chitosan (30 m/z), (d) nitrogen containing fragments from chitlacA (58 m/z) and (e) sodium ions. All images were normalized to the total ion image (f).

The chitlac coating on PCL surface was investigated by ToF-SIMS and multivariate analysis (PCA). This approach was used to differentiate between physical and chemical contribution to the coating procedure. During a coating procedure the physisorption and chemisorption are virtually always involved, even if a covalent modification is expected for a mechanism of immobilization [11]. In this study, chitlac coatings on the untreated PCL and hydrolyzed PCL were compared. In

the first case, the coating mechanism should be driven mostly by weak forces. In the second case, chitlac should be covalently attached *via* amide bond formation to hydrolyzed and carboxylated PCL surface. This should guarantee a better immobilization of chitlac.

The peak list used as dataset for principal component analysis was obtained by the combination of characteristic PCL and chitlac fragments. In fact, on the basis of mapping results, it was expected that the detected fragments should derive from PCL or chitlac. Positive polarity was chosen because a large number of peaks were identified, especially nitrogen containing fragments.

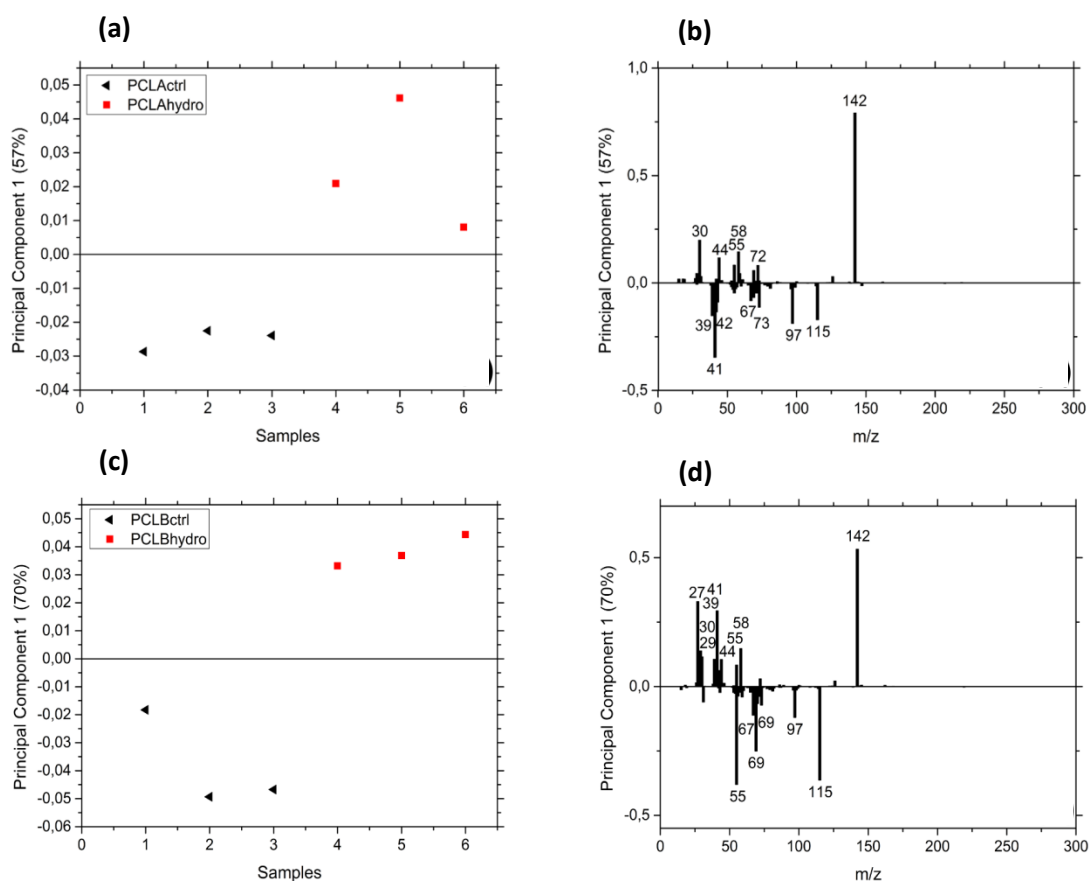


Figure 3.8: PC1 (57% variance) (a) loadings and (b) scores plots for positive ions from PCA processing of ToF-SIMS spectra over the mass range from m/z 1 to 300 for PCLActrl and PCLAhidro. PC1 (70% variance) (c) loadings and (d) scores from PCA data reduction of positive ToF-SIMS spectra over the mass range from m/z 1 to m/z 300 for PCLBctrl and PCLBhydro.

In figure 3.8a and 3.8b, PC1 scores and loadings plot for PCL control and hydrolyzed, functionalized with chitlacA (respectively PCLActrl and PCLAhidro samples) are shown. PC1 scores reported that the two sets of samples were clearly different, consistent with the fact that hydrolysis treatment changed PCL surface.

PC1 loadings plot showed which masses were responsible of separation between PCLActrl and PCLAhydro. In particular, it was possible to appreciate that the variables with negative loadings value m/z 41($C_3H_5^+$), 42($C_3H_6^+$), 43($C_2H_3O^+$), 67($C_5H_7^+$), 73($C_4H_9O^+$), 97($C_5H_5O_2^+$) and 115($C_6H_{11}O_2^+$) were associated to known fragmentations of substrate (PCL). On the other hand, nitrogen containing fragments at m/z 30(CH_4N^+), 44($C_2H_6N^+$), 55($C_3H_3O^+$), 58($C_3H_8N^+$), 72($C_3H_6NO^+$) and 142($C_7H_{12}NO_2^+$) were correlated with PCL functionalized (PCLAhydro).

PCL peaks at m/z 41, 97 and 115 were related to PCLActrl. On the contrary, chitosan and chitlac peaks at m/z 30, 44, 58 and 142 were associated to PCLAhydro. ToF-SIMS spectra confirmed the presence of chitlac on both untreated and hydrolyzed samples. From loadings plot, it was possible to obtain information regarding the peaks intensity distribution. In this case, chitlac characteristic peaks were strictly related to the hydrolyzed PCL surface suggesting a better distribution of chitlac signals after the introduction of surface carboxylic groups.

In the same way, in figure 3.8c and 3.8d, PC1 loadings and scores plot for PCL and hydrolyzed PCL surface, functionalized with chitlacB (reported as PCLBctrl and PCLBhydro samples) are displayed.

Negative loadings at m/z 55 ($C_3H_3O^+$), 69 ($C_5H_9^+$), 97($C_5H_5O_2^+$), 115($C_6H_9O_2^+$) were identified as fragments correlated with PCLBctrl. Positive loadings at m/z 27($C_2H_3^+$), 29($C_2H_5^+$), 30(CH_4N^+), 41($C_3H_5^+$), 55($C_4H_7^+$), 58($C_3H_8N^+$) and 142($C_7H_{12}NO_2^+$) were associated with PCLBhydro.

Also in this case, while PCL fragment ions were correlated to PCLBctrl, chitosan and chitlac fragment ions were associated to PCLBhydro.

ToF-SIMS analysis along with PCA have confirmed the same results showed for chitlacA functionalization. In both cases, the ion with higher loadings value at m/z 142, which was predominant in chitlac spectrum, was responsible for the grouping of chitlac samples deposited onto hydrolyzed PCL surface.

The same peak list including typical fragments of PCL and chitlac, in the mass range from m/z 1 – 300, was adopted for a biplot graphic display.

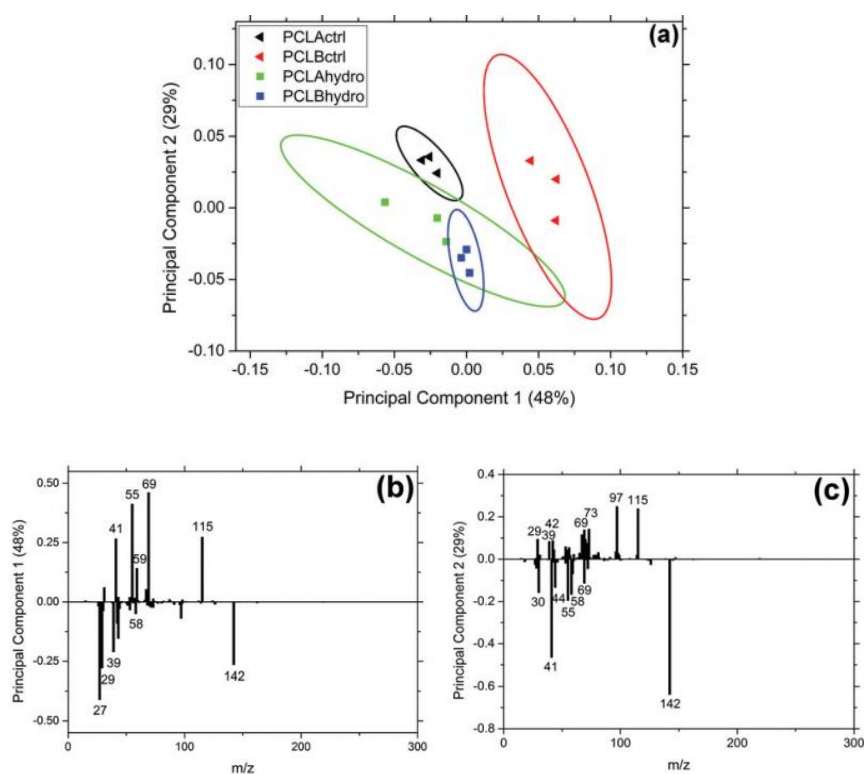


Figure 3.9: (a) Scores cross-plot of PC1 (48% variance) vs PC2 (29% variance); (b) loadings plots of PC1 (b) and PC2 (c) of positive ToF-SIMS spectra from treated samples with chitlacA and chitlacB and their respective controls.

Score cross-plot (PC1 vs PC2) and associated loadings plots for positive spectra from control and treated samples, are shown in Fig. 3.9. In the score plot Fig. 3.9(a), where ellipses represent 95% confidence intervals, PC1 separated PCLBctrl and PCLBhydro from PCLActrl and PCLAhydro. In particular, PCLBctrl was mainly separated from the rest of the scores. Loadings plot of PC1 and PC2 shows the variables responsible of sample separation between control and treated samples. PC1 and PC2 together account for 77% of the total variance.

The PC1 loadings in Fig. 3.9(b) indicated that this unexpected location in the PCA score plot was due to a greater presence of PCL substrate signals. This suggests a weaker physisorption effect for untreated PCL surface in the case of interaction with lower lactosilated chitosan (chitlacB). On the other hand, the PC1 negative loadings indicated that the rest of the scores was strictly related to the chitlac presence.

The second principal component (PC2) well separated the control samples (PCLActrl and PCLBctrl) from their respective treated samples (PCLAhydro and PCLBhydro) as shown in Fig. 3.9(a). The negative PC2 loadings corresponded to the peaks coming from chitlac fragmentation Fig. 3.9(c). The molecular fragment at m/z 142 ($C_7H_{12}NO_2^+$) is correlated with the hydrolyzed samples. As expected, the scores and loadings plots are in agreement with the previous results reported (Fig. 3.8), in which chitlac with two different degrees of derivatization were individually

evaluated. Taken together, these findings highlight the successful chemical immobilization of chitlac onto poly(ϵ -caprolactone) activated substrates.

3.3.6 Evaluation of grafting yield of chitlac A and B

To determinate the immobilization yield of the two variants of chitlac (A and B), a peaks *ratio* analysis was carried out. For this analysis, the following *ratio* was used:

$$Ratio = \frac{\Sigma I_{chitlac}}{\Sigma I_{PCL}} \quad \text{Eq. (3.1)}$$

Where the terms in this equation were defined as followed:

- $\Sigma I_{chitlac}$ was the sum of characteristic chitlac peaks area.
- ΣI_{pcl} was the sum of peaks area of the two high molecular weight fragments of PCL backbone.

This peaks *ratio* analysis was calculated for PCLActrl, PCLAhydro, PCLBctrl and PCLBhydro samples (fig. 3.10). Peaks at m/z 97($C_5H_5O_2^+$) and 115($C_6H_{11}O_2^+$) were considered to identify PCL. Peaks at m/z 42($C_2H_4N^+$), 44($C_2H_6N^+$), 46($C_2H_8N^+$), 58 ($C_3H_8N^+$), 73 ($C_3H_5O_2^+$) and 86 ($C_4H_8NO^+$) were used as characteristic of chitlac. As a further normalization, each hydrolyzed sample (PCLAhydro and PCLBhydro) was normalized against its own control (PCLActrl and PCLBctrl, respectively).

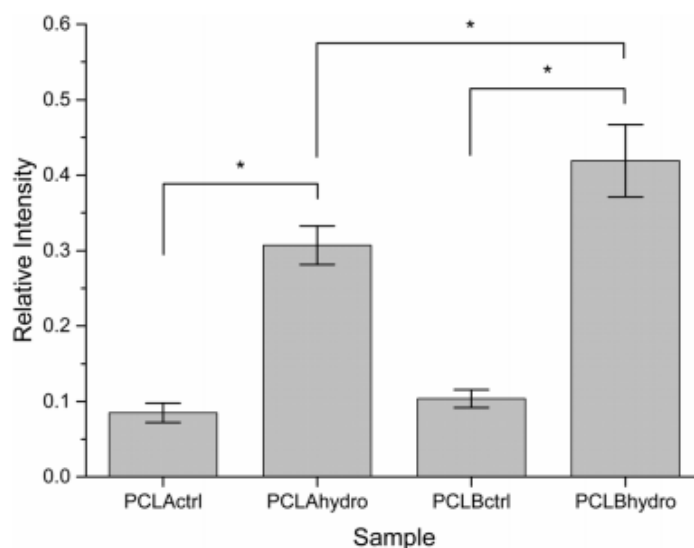


Figure 3.10: *Ratio* between $\Sigma I_{chitlac}$ and ΣI_{pcl} for PCLActrl, PCLAhydro, PCLBctrl, and PCLBhydro samples ($p = 1.3 \times 10^{-6}$). Asterisk denotes significance.

Samples	Ratio	SD	Ratio hydro/ctrl
PCLA ctrl	0.085	0.013	3.614
PCLA hydro	0.307	0.026	
PCLB ctrl	0.104	0.012	4.038
PCLB hydro	0.419	0.048	

Table 3.3: Different ratios for control or treated PCL, functionalized with chitlacA or chitlacB.

As showed in figure 3.10 and table 3.3, the *ratio* for the PCL samples underwent hydrolysis treatment was always higher than the samples where the chitlac was deposited onto the untreated PCL surface.

Normalized values (“hydro/ctrl” values in Table 3.3) evidenced how immobilization yield for chitlacB was higher than for chitlacA. This result could be explained in light of the higher number of free amines available for reaction with PCL surface carboxyl groups in the case of lower lactosilated chitosan (chitlacB).

3. 4 Conclusions

In this study, a new functionalization of poly(ϵ -caprolactone) (PCL) with lactose-modified chitosan (chitlac) attachment has been presented, using as the activation method of the substrate, the alkaline hydrolysis. Each step of PCL functionalization was investigated by ToF-SIMS, as a high vacuum sensitive surface analysis technique, coupled to univariate and multivariate (PCA) statistical analysis.

High-resolution mass spectra revealed a modification in the surface chemistry of PCL membrane after base-catalyzed hydrolysis treatment, with an increase in carboxyl group content, necessary for the further covalent grafting of chitlac.

After the step of polysaccharide grafting, first, ToF-SIMS mapping evidenced the homogeneous distribution of chitlac on PCL surface, validating alkaline hydrolysis as a facile method to modify PCL surface and to increase the efficiency of subsequent grafting of polysaccharides. Second, the coupling of ToF-SIMS and PCA, permitted to assert a greater functionalization yield of samples, underwent hydrolysis, than the control ones, where chitlac was only physisorbed.

Furthermore, ToF-SIMS positively discriminated between two different chitlac variants (chitlacA and chitlacB) characterized by different derivatization degree, pointing at a higher immobilization yield for the low-derivatized chitlacB, caused by its higher number of free amines.

In conclusion, ToF-SIMS and PCA can be successfully applied to the characterization of PCL surface chemistry, evidencing changes in the biopolymer surface following base-catalyzed hydrolysis treatment.

3.5 References

- [1] A. B Faia-Torres, S. Guimond-Lischer, M. Rottmar, M. Charnley, T. Goren & K. Maniura-Weber. Differential regulation of osteogenic differentiation of stem cells on surface roughness gradients. *Biomaterials*, 35(33), 9023-9032, 2014.
- [2] I. Donati, S. Stredanska, G. Silvestrini, A. Vetere, P. Marcon, E. Marsich & F. Vittur. The aggregation of pig articular chondrocyte and synthesis of extracellular matrix by a lactose-modified chitosan. *Biomaterials*, 26(9), 987-998, 2005.
- [3] A. Rainer, P. Mozetic, S.M. Giannitelli, D. Accoto, S. De Porcellinis & E. Guglielmelli. Computer-aided tissue engineering for bone regeneration. Biomedical Robotics and Biomechatronics (BioRob), in: 2012 4th IEEE RAS & EMBS International Conference on: IEEE, 473–476, 2012.
- [4] H. Sun, G. Xu. *Polymer Preprints* 52, 325-326, 2011.
- [5] E Rosellini, C. Cristallini, G.D. Guerra, & N. Barbani. Surface chemical immobilization of bioactive peptides on synthetic polymers for cardiac tissue engineering. *Journal of Biomaterials Science, Polymer Edition*, 26(9), 515-533, 2015.
- [6] S. Roberson, A. Sehgal, A. Fahey, & A. Karim. Time-of-flight secondary ion mass spectrometry (ToF-SIMS) for high-throughput characterization of biosurfaces. *Applied surface science*, 203, 855-858, 2003.
- [7] J. S. Fletcher, X. A. Conlan, E. A. Jones, G. Biddulph, N. P. Lockyer, & J. C. Vickerman. TOF-SIMS analysis using C60. Effect of impact energy on yield and damage. *Analytical chemistry*, 78(6), 1827-1831, 2006.
- [8] M. Chen, & F. Besenbacher, Light-driven wettability changes on a photoresponsive electrospun mat. *ACS nano*, 5(2), 1549-1555, 2011.
- [9] M. Dubey, K. Emoto, F. Cheng, L. J. Gamble, H. Takahashi, D. W. Grainger, & D.G. Castner. Surface analysis of photolithographic patterns using ToF-SIMS and PCA. *Surface and Interface Analysis*, 41(8), 645-652, 2009.

[10] P. M. López-Pérez, R. M. da Silva, C. Serra, I. Pashkuleva, & R. L. Reis. Surface phosphorylation of chitosan significantly improves osteoblast cell viability, attachment and proliferation. *Journal of Materials Chemistry*, 20(3), 483-491, 2010.

[11] M. Aslam, A. Dent. Bioconjugation-protein coupling techniques for the biomedical sciences. Macmillan Reference Ltd, 505, 1998

Chapter 4

Functionalization of titanium and Ti6Al4V substrate with chitosan by carboxyl groups as linker agent

A new method of chitosan covalent grafting on titanium and Ti6Al4V alloy was studied using the carboxyl group as agent linker.

Moreover, metal surfaces were undergone various pretreatments, in particular, focusing on the acid etching (HCl, HF and H₂SO₄/H₂O₂), to evaluate the treatment which allowed the best chitosan functionalization efficiency. To obtain carboxyl groups on metal surfaces, the samples of titanium or alloy were immersed in a solution of chloroacetic acid, as shown in fig. 4.1, step 1.

The chitosan was grafted onto the titanium and alloy surfaces employing the 1-ethyl-3-(3-dimethylaminopropyl) carbodiimide hydrochloride (EDC) and the N-hydroxysuccinimide (NHS) as coupling agents, to activate the reaction between the carboxyl groups of titanium and the amino group of chitosan (Figure 4.1).

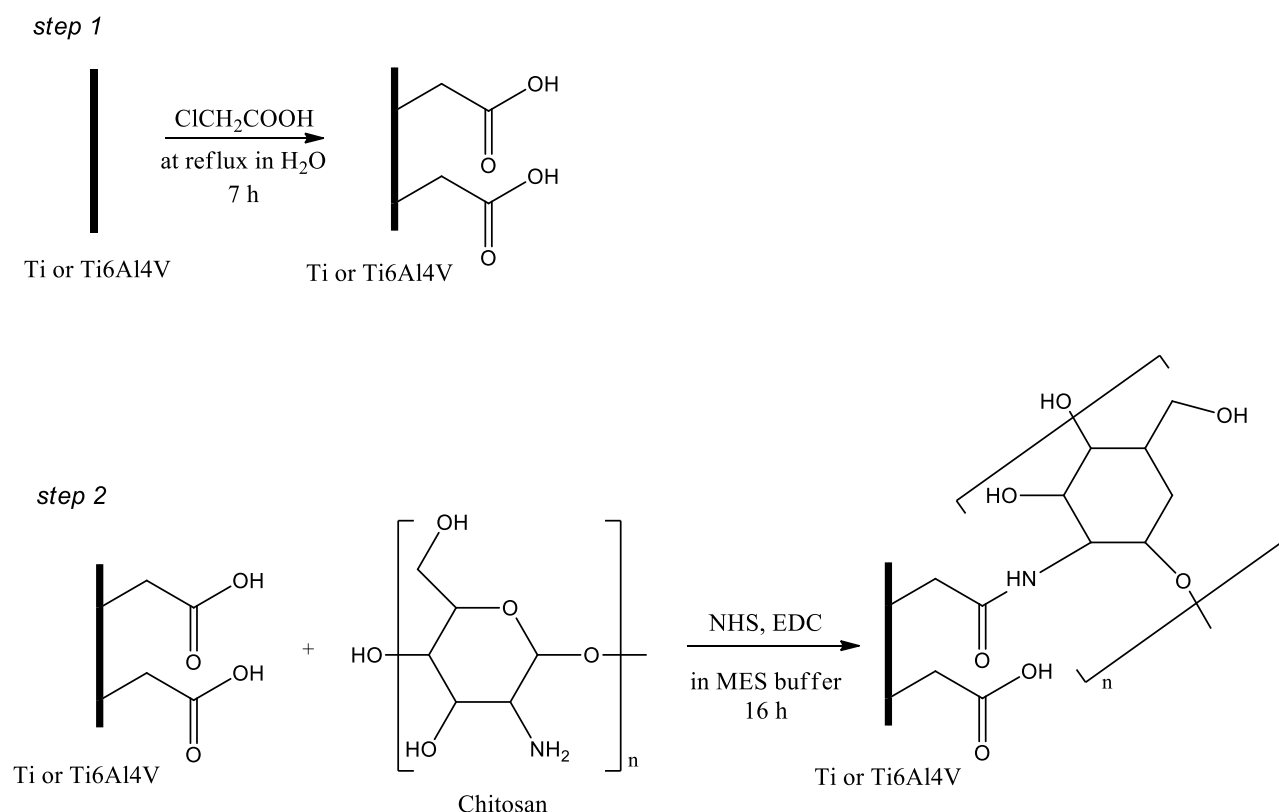


Figure 4.1: Carboxylation of titanium or Ti6Al4V surfaces and immobilization of chitosan.

Every step of functionalization was characterized by Fourier Transform Infrared Spectrometry (FTIR) and X-ray Photoelectron Spectroscopy (XPS). In addition, the chitosan grafting on the carboxylated surfaces was evaluated by the Cyclic Voltammetry. Moreover, by this electroanalytical method, the stability of covalent chitosan coating was verified, compared to the samples where chitosan was only physisorbed on the metal surface.

4.1 MATERIALS

Titanium foils (0.127 mm thickness, purity 99.7%), chitosan with medium molecular weight (75-85% deacylated), 1-ethyl-3-(3-dimethylaminopropyl) carbodiimide (EDC), the N-hydroxysuccinimide (NHS), 2-(N-morpholino)ethanesulfonic acid (MES, 0.1M, pH=6.20), potassium ferricyanide(II) $K_4Fe(CN)_6$, potassium ferricyanide (III) $K_3Fe(CN)_6$, KCl, HCl and HF solutions were purchased from Sigma Aldrich (Milwaukee, WI).

Grade 5 Ti6Al4V alloy sheets of 0.4 mm thickness were supplied by Ti-shop.com. All reagents were used without further purification.

4.1.1 Preliminary preparation of substrates

Titanium and Ti6Al4V sheets were cut into 1cm x 1cm pieces.

Ti6Al4V foils was preliminary cleaned with an acetone dipped adsorbent paper and later washed with water and polished using a 1200 grid sandpaper.

All samples were cleaned in an ultrasonic bath first with water/ acetone solution (v/v, 50/50) for 10 minutes and then other 10 minutes in ethanol.

4.1.2 Substrate Pretreatments

The titanium and Ti6Al4V alloy samples (Table 4.1) were exposed to different treatments (A, B, C, D and E as explained below) before the carboxylation reaction.

A: Substrate with no previous pretreatment;

B: Substrate was immersed in aqueous solution of HCl (18 wt%) at 80°C for 10 minutes and later it was washed with water and dried at room temperature.

C: Substrate was immersed in an aqueous solution of HF (2.5 wt%) for 45 seconds. Later, it was washed with water and dried at room temperature.

D: Substrate was heated at 400 °C for 4 hours to stabilize the oxide layer on the surface.

E: Substrate was treated at 25° for 2 hours with a solution consisting of equal volume concentrated

H₂SO₄ and 30% aqueous H₂O₂. [1]

4.1.3 Carboxylation of titanium and Ti6Al4V alloy surface

The activation of titanium/Ti6Al4V surface with the carboxyl group was performed immersing the samples in an aqueous solution of chloroacetic acid (ClCH₂COOH, 0.1 M) at reflux for 7 h; then the sample was repeatedly washed with deionized water until the pH value of the mixture became neutral and dried for 24 hours at 80°C [2].

4.1.4 Grafting of chitosan on carboxylated samples

The carboxylated samples were treated in a solution of chitosan (10 mg/mL), 2-ethyl-3-(3-dimethylaminopropyl)carbodiimide (EDC; 20mM), N-hydroxysuccinimide (NHS; 50 mM) in 2-(N-morpholino) ethanesulfonic acid (MES) buffer (pH= 6.0) at room temperature for 16 h [3]. Covalent coupling was obtained through the reaction between carboxyl groups of titanium/alloy substrate and free amino groups of chitosan. Finally, samples were rinsed with MES buffer followed by water in order to remove non-grafted molecules and dried for 12 h.

4.1.5 Chitosan physisorption on titanium and Ti6Al4V alloy

The titanium and Ti6Al4V alloy samples, pretreated by HCl without linker, were immersed in a solution of chitosan (10 mg/mL) in 2-(N-morpholino) ethanesulfonic acid (MES) buffer (pH= 6.0) at room temperature for 16 h.

Then, the sample was rinsed with MES buffer followed by water in order to remove non physisorbed molecules and dried for 12 h at room temperature.

Table 4.1 reports titanium and Ti6Al4V label samples.

Sample Name		Treatment	Step process
Ti(A)	Ti6Al4V(A)	A	Starting sample
Ti(A)_linker	Ti6Al4V(A)_linker		Starting sample + carboxyl group
Ti(A)_chitosan	Ti6Al4V(A)_chitosan		Starting sample + carboxyl group + chitosan
Ti(B)	Ti6Al4V(B)	B	Starting sample
Ti(B)_linker	Ti6Al4V(B)_linker		Starting sample + carboxyl group
Ti(B)_chitosan	Ti6Al4V(B)_chitosan		Starting sample + carboxyl group + chitosan
Ti(B)_physis	Ti6Al4V(B)_physis		Starting sample + chitosan
Ti(C)	Ti6Al4V(C)	C	Starting sample
Ti(C)_linker	Ti6Al4V(C)_linker		Starting sample + carboxyl group
Ti(C)_chitosan	Ti6Al4V(C)_chitosan		Starting sample + carboxyl group + chitosan
Ti(D)	Ti6Al4V(D)	D	Starting sample
Ti(E)	Ti6Al4V(E)	E	Starting sample

Table 4.1: Titanium and Ti6Al4V Samples Nomenclature

4.2 METHODS

4.2.1 Scanning electron microscope (SEM)

The surface morphologies of untreated, HCl and HF etched titanium and Ti6Al4V, were examined using a scanning electron microscope (SEM, Philips XL30, The Netherlands).

4.2.2 Fourier Transform Infrared Spectrometry (FTIR-ATR)

FTIR spectra were recorded on a Thermo Scientific Nicolet iN10 FTIR spectrometer fitted with a liquid nitrogen-cooled MCT detector with a spectral range from 4000 cm^{-1} to 675 cm^{-1} , by the attenuated total reflection (ATR) technique for all sample, except for the chitosan standard, which was acquired in transmission mode. For each sample, at least five measurements were acquired from different areas, with a scanning area of 80 μm x 80 μm . Each FTIR spectrum was an average of 64 scans, with a 8 cm^{-1} resolution. Thermo Scientific Omnic software was used for post elaboration spectra. For each spectrum, automatic atmospheric suppression and automatic baseline correction were performed.

4.2.3 X-ray Photoelectron Spectroscopy (XPS) characterization

X-ray Photoelectron Spectroscopy studies were performed using an instrument designed by Science Department in RomaTre, consisting of preparation and analysis chambers separated by a gate valve.

The analysis chamber was equipped with six degrees of freedom manipulator and a 150 mm mean radius hemispherical electron analyzer with five-lens output system combined with a 16-channel detector. MgK alpha non-monochromatized X-radiation ($h\nu = 1253.6$ eV) was used for recording the Ti2p, O1s, C1s, N1s core level spectra for each sample. The electron energy analyzer was operated with a pass energy of 25 eV enabling high resolution of the spectra to be obtained; furthermore, a step size of 0.1 eV was employed.

A curve-fitting analysis of the C1s and O1s spectra was performed; gaussian curves were used as fitting functions (typical full width at halfmaximum in the range 1.7-2.1 eV) after subtraction of a Shirley-type background.

The analyzed spectra were energy referenced to the C1s signal of aliphatic C-C carbons located at 285.0 eV of Binding Energy (BE) [4]. Atomic ratios were calculated from peaks areas using Scofield's cross as section sensitivity factors.

4.2.4 Cyclic voltammetry characterization

Voltammetric measurements were performed with an Amel System 5000 in a three electrodes cell. Acquisition software was a CorrWare version 3.5c Scribner; elaboration software was a CorrView version 3.5c Scribner.

Titanium (Ti(A), Ti(B) and Ti(C)), titanium modified by chitosan (Ti(A)_chitosan, T(B)_ chitosan, Ti(C)_chitosan), Ti6Al4V (Ti6Al4V(A), Ti6Al4V(B), Ti6Al4V(C)), Ti6Al4V modified by chitosan (Ti6Al4V(A)_chitosan, Ti6Al4V(B)_chitosan, Ti6Al4V(C)_chitosan), Ti(B)_physis and Ti6Al4V(B)_physis were employed as working electrode (area 1 cm²) using a platinum counter electrode and a Ag/AgCl reference electrode.

Cyclic voltammograms (CVs) of the Fe(CN)₆^{3-/4-} redox couple were recorded in solution of KCl (0.1 M) containing 1 mM of K₃Fe(CN)₆ and 1 mM of K₄Fe(CN)₆ at a rate scan of 50 mV/s.

4.3 RESULTS AND DISCUSSIONS

4.3.1 SEM characterization: study of the effect of HCl and HF etching treatments on titanium and Ti6Al4V surfaces

Scanning electron microscope SEM was used to evaluate the different effects of etching treatments on the titanium and Ti6Al4V surfaces, in terms of morphology and roughness [5].

The analysis of surface morphologies showed that the HCl pretreated titanium (Ti(B), fig. 4.2(a)) presented an increase roughness compared to the untreated one (Ti(A), fig. 4.2(b)), but the initial aspect was substantially the same. The evident linear stripes may be attributed to the cutting method used to create the titanium foils.

Instead, as can be seen in Fig. 4.2 (c), the SEM image of the titanium surface after etching in HF showed a significantly rougher surface than the untreated sample, due to the removal of some titanium atomic layers.

The removal appeared to be not isotropic, highlighting (inset of Fig. 4.2c) excavations of polyhedral shape which recall the hexagonal close-packed structure typical of titanium crystal [6].

For the Ti6Al4V alloy, the untreated surface appeared rougher, than the untreated titanium surface sample. Furthermore, no difference was evident between the untreated and the HCl pretreated alloy (respectively reported in figure 4.2 b and d). For the HF pretreated alloy (fig. 4.2(f)), the surface was rougher than untreated and HCl pretreated samples, probably due to the aggressiveness of the HF etching treatment.

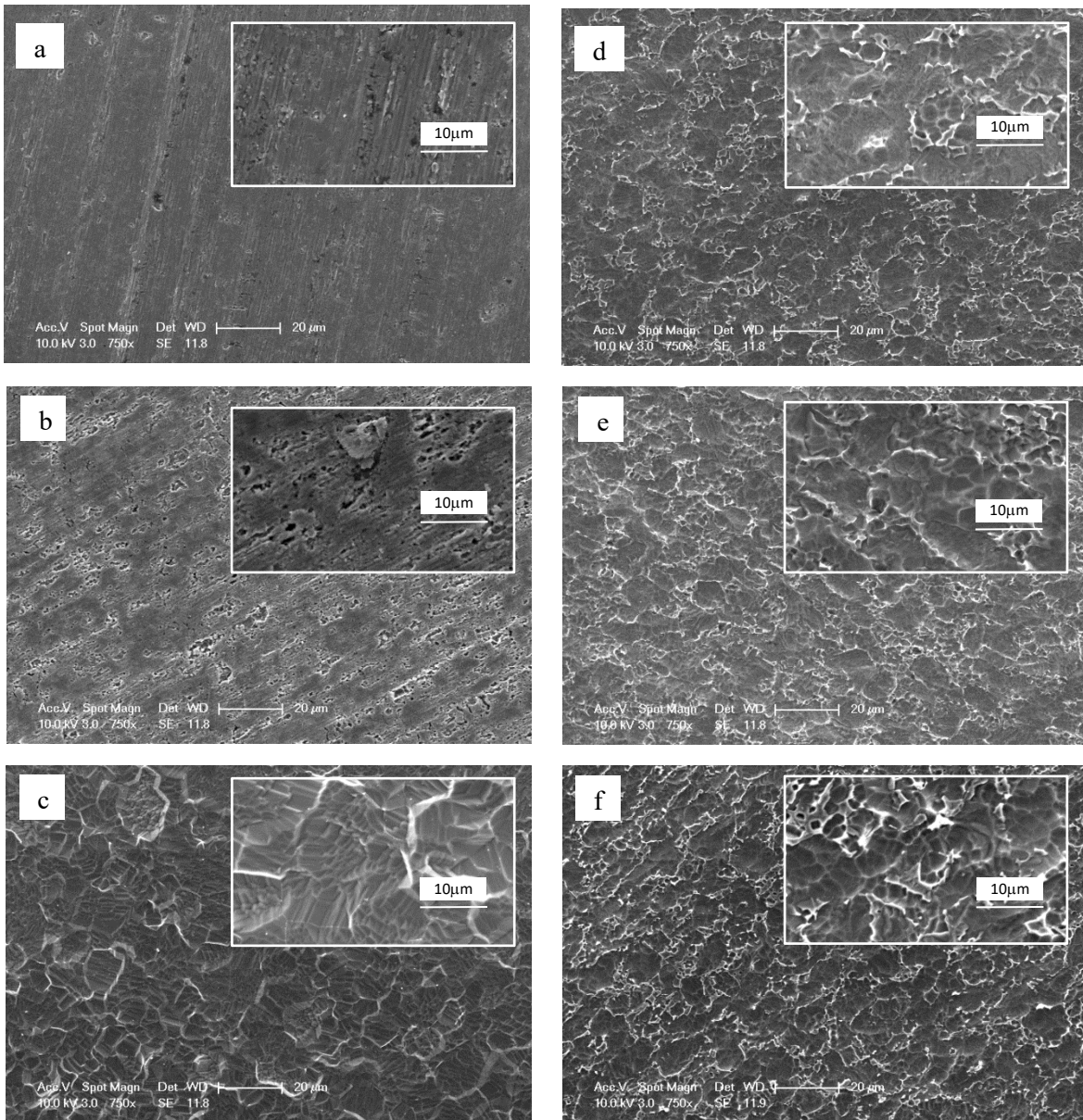


Figure 4.2: SEM images of untreated titanium (a), etched titanium with HCl (b) and HF (c); untreated Ti6Al4V (d), etched Ti6Al4V with HCl (e) and HF (f) at 750× and 3000× (inset)

4.3.2 FTIR-ATR analysis

In order to illustrate clearly the surface functionalization of metal surface with the linker agent (-COOH) (fig 4.1, step 1) and the grafting of chitosan (fig. 4.1, step 2), FTIR-ATR analysis was used.

4.3.2.1 Carboxylation of titanium surfaces

The presence of carboxyl groups on titanium surfaces was essential for the subsequent immobilization of chitosan.

In figures 4.3a, 4.3b and 4.3c, the spectra are relative to carboxylation of Ti(A)_linker, Ti(B)_linker and Ti(C)_linker samples. The analyzed spectral range was between 4000 cm^{-1} to 1500 cm^{-1} , where characteristic absorptions of COOH group should be present.

In all three samples, the untreated and the HCl and HF pretreated ones, FTIR spectra highlighted the presence of the carboxyl group due to the stretching of C=O ($\sim 1728\text{ cm}^{-1}$); the bands around 2920 cm^{-1} are characteristic of C-H stretching. The weak peak around 3400 cm^{-1} could be explained by the stretching of O-H from the water molecules absorbed on the surface as reported in literature [2]. This was in contrast to the reference sample spectra (respectively Ti(A), Ti(B), and Ti(C)) where these bands at 1728 and 2920 cm^{-1} were absent.

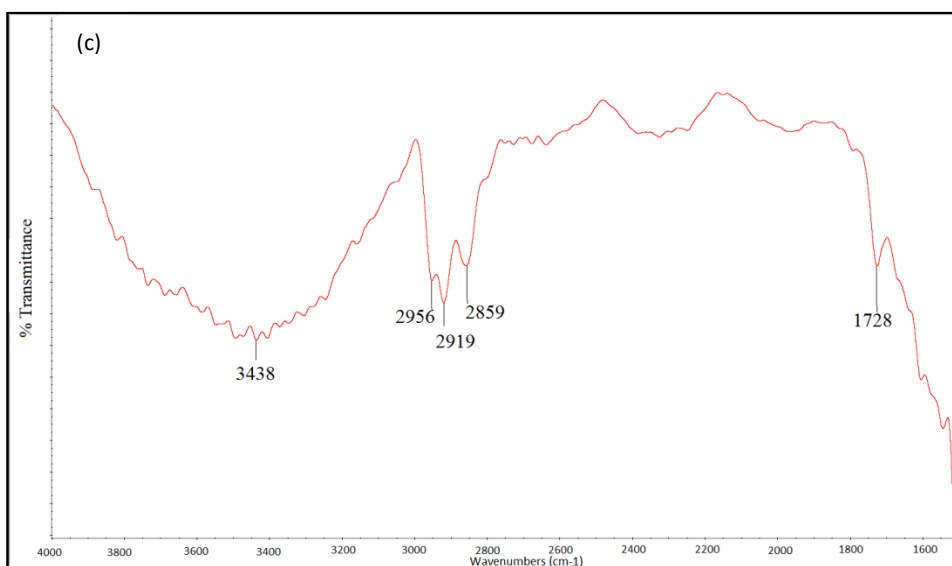
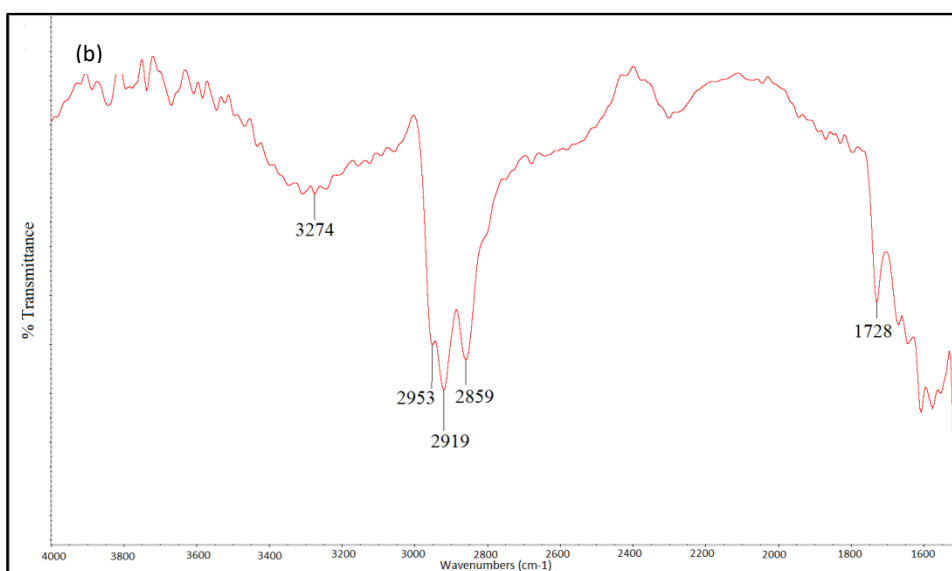
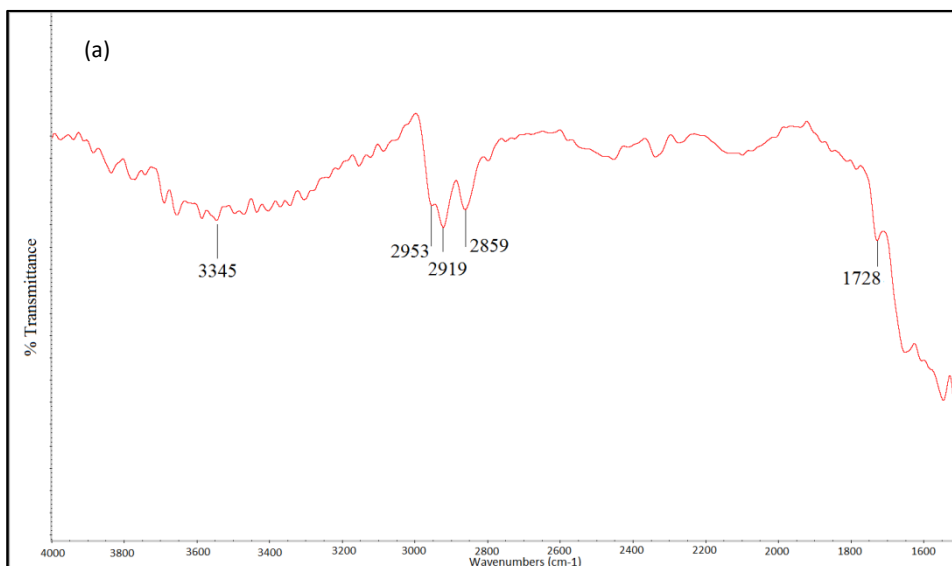


Figure 4.3: FTIR spectra of carboxylated: (a) untreated titanium (Ti(A)_linker); (b) HCl pretreated titanium (Ti(B)_linker) and (c) HF pretreated titanium (Ti(C)_linker)

The bond of carboxyl groups on titanium surface results to be robust. Indeed, by FTIR-ATR analysis, it was possible to verify that the spectrum of the sample Ti(C), which was further cleaned in water by ultrasound for 10 minutes, presented the same bands of that one simply wash by distilled water.

In spectra of the samples of Ti heated for 4 hours at 400°C (Ti(D)) and pretreated by the solution of H₂SO₄/ H₂O₂ (Ti(E)), after carboxylation (step 1, fig. 4.1), no evidence of carboxylation group was revealed. There was no difference between the spectra of the samples, before and after the carboxylation procedure.

In summary, FTIR spectra, relative to samples, obtained after carboxylation reaction, showed that only in the untreated, HCl and HF pretreated samples, carboxyl group seemed to immobilized on the titanium surface. It can be possible to observe the same good results if the carboxylation took place on a native TiO₂ titanium surface or on HCl and HF treated ones.

4.3.2.2 Chitosan grafting on carboxylated titanium surface

To evaluate the chitosan attachment to the carboxylated samples, an IR spectrum of the chitosan powder used as reactant in step 2, fig. 4.1, was acquired in transmission mode. Figure 4.4 shows the characteristic bands of chitosan: in detail the large band at around 3300 cm⁻¹ corresponded to the overlapping of the O-H stretching and N-H stretching vibration. Instead, the band at 2878 cm⁻¹ corresponded to C-H₂ stretching vibration, while bands at 1655, 1578, 1376 and 1319 cm⁻¹ were attributed respectively to the C=O stretching of amide, N-H bending vibration, the C-H bending and the C-N stretching. The bands at 1150, 1030 and 896 cm⁻¹ were assigned to skeleton vibration of chitosan structure [7].

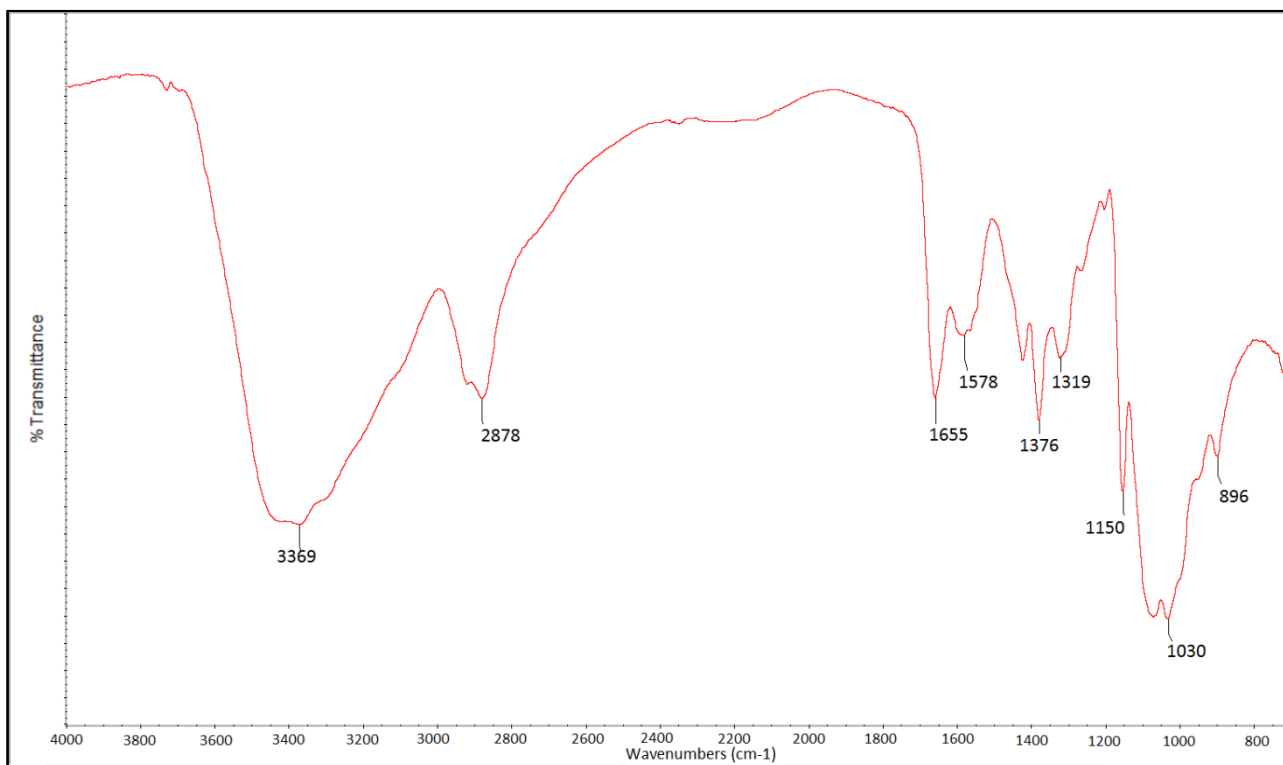


Figure 4.4: FTIR spectrum of chitosan

The success of the chitosan grafting on carboxylated samples could be ascertained by comparing the chitosan IR spectrum with spectra of Ti(A)_chitosan (a), Ti(B)_chitosan(b), Ti(C)_chitosan (c) shown in figure 4.5. The spectra ((b) and (c)) of titanium samples pretreated by HCl and HF presented the characteristic bands of chitosan. On the contrary, in the spectrum of the untreated sample Ti(A)_chitosan, it was difficult to distinguish all typical bands of chitosan.

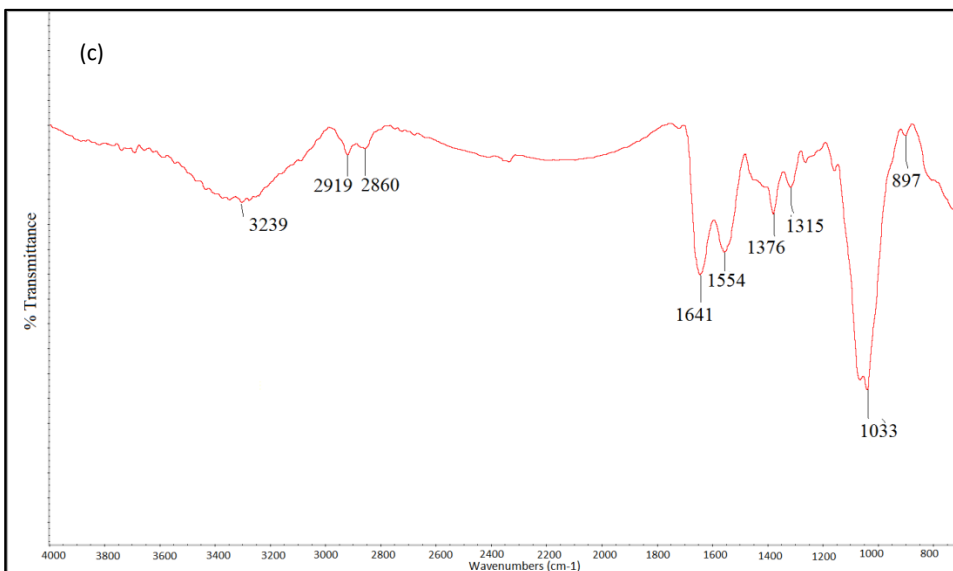
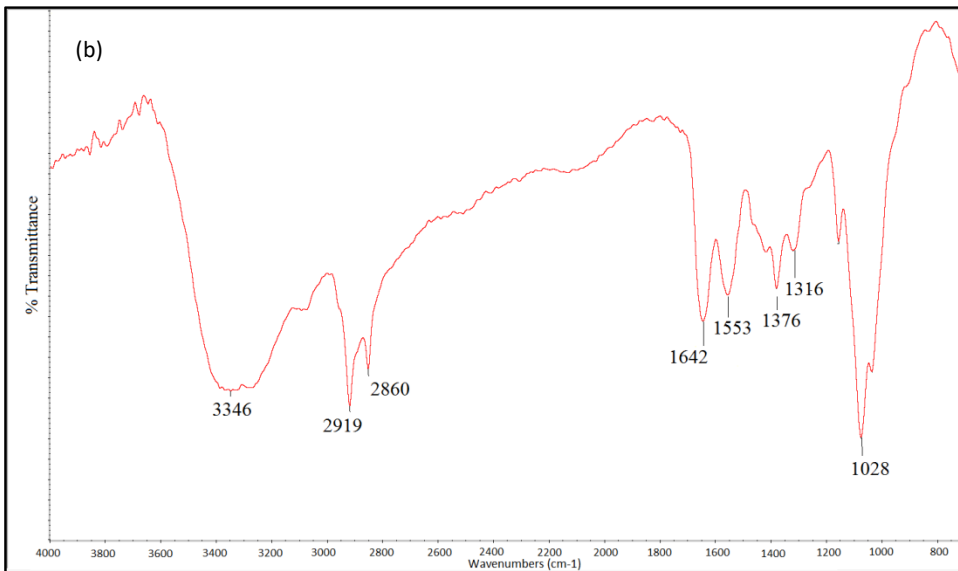
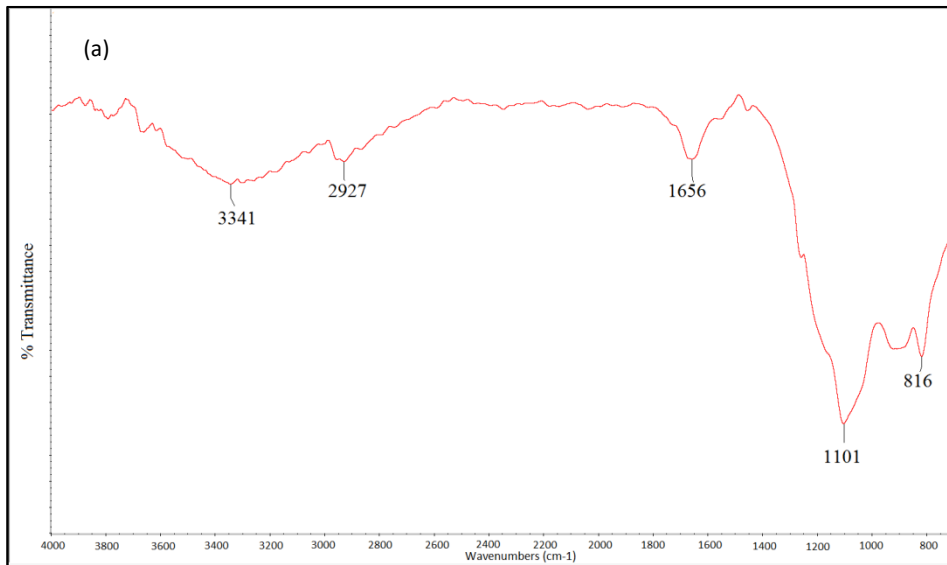


Figure 4.5: FTIR spectra after chitosan grafting procedure of carboxylated untreated titanium (Ti(A)_chitosan, (a)), HCl pretreated titanium (Ti(B)_chitosan, (b)), HF pretreated titanium (Ti(C)_chitosan (c)).

Moreover, the formation of bond between chitosan and carboxyl groups could be confirmed by FTIR analysis as reported in literature [8]. The spectrum of chitosan standard (fig. 4.6a) showed the bands of amide connection at 1655 cm^{-1} and 1578 cm^{-1} . In the spectrum of Ti(B)_chitosan surface (fig. 4.6b) these peaks was slightly shifted to 1642 cm^{-1} and 1553 cm^{-1} respectively.

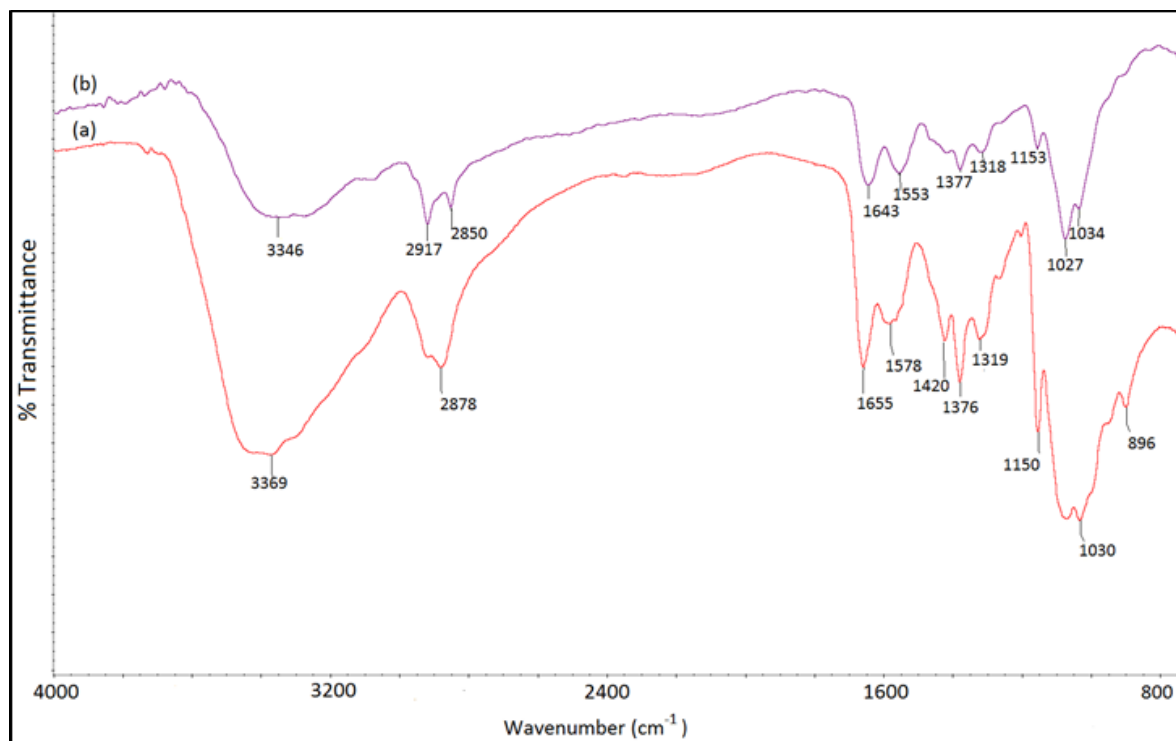


Figure: 4.6: FTIR-ATR spectra. (a) Chitosan (b) Ti(B)_chitosan

4.3.2.3 Carboxylation of Ti6Al4V surfaces

The carboxylation procedure and then the chitosan grafting, were tested on Ti6Al4V alloy. In detail, the carboxylation reaction was performed on the untreated Ti6Al4V surface, the HCl and the HF pretreated ones (respectively A,B and C treatments), keeping in mind the good results obtained on titanium sample with the same pretreatments.

FTIR spectra confirmed the presence of COOH groups, also in the case of Ti6Al4V alloy. Indeed, the spectra (a), (b) and (c) in figure 4.7 of Ti6Al4V(A)_linker, Ti6Al4V(B)_linker and Ti6Al4V(C)_linker, showed the characteristic band of the stretching of C=O at $\sim 1728\text{ cm}^{-1}$ and the C-H methylene group at $\sim 3000\text{ cm}^{-1}$.

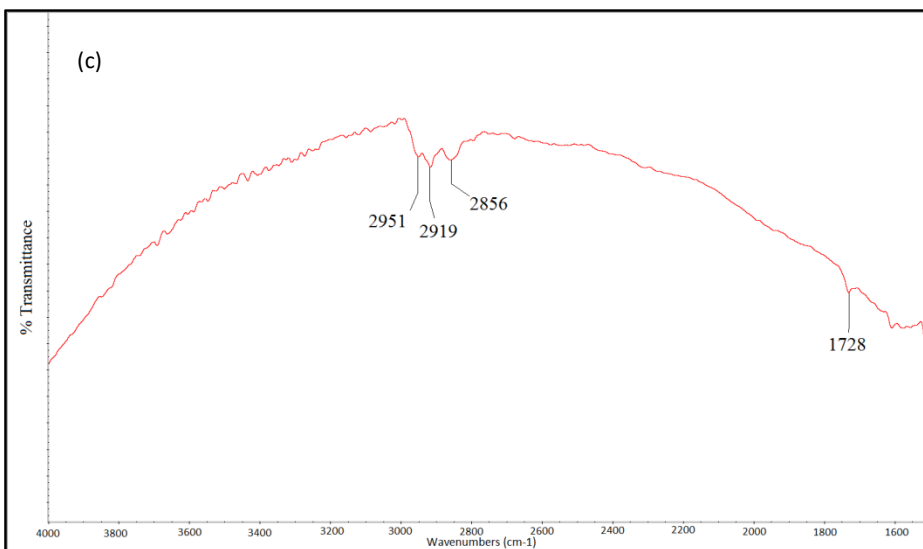
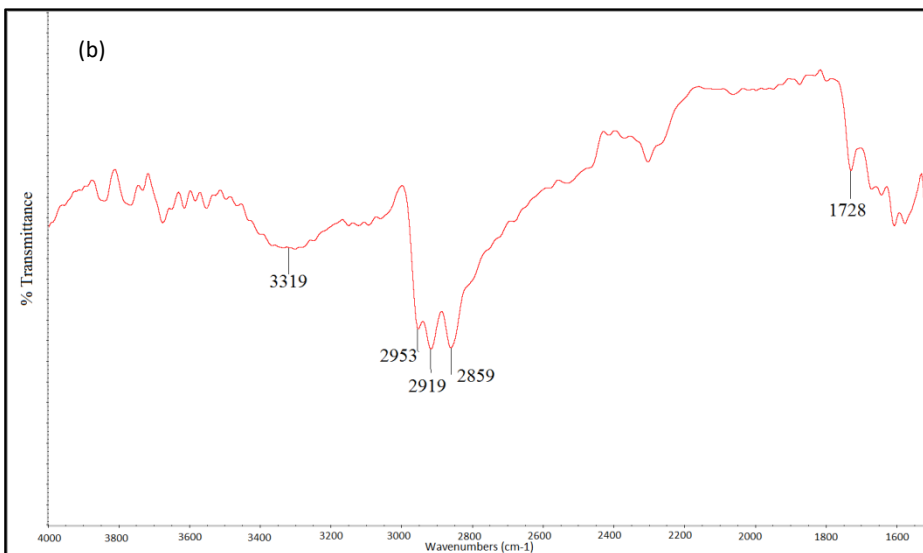
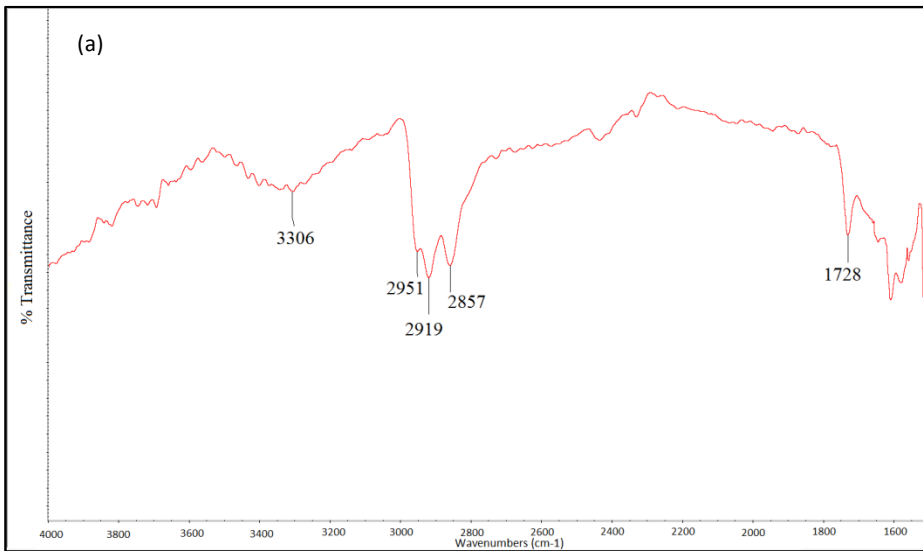


Figure 4.7: FTIR spectra after carboxylation procedure of untreated alloy (Ti6Al4V(A)_linker) (a) and HCl pretreated alloy (Ti6Al4V(B)_linker) (b) and HF pretreated alloy (Ti6Al4V(C)_linker) (c)

4.3.2.4 Chitosan grafting on the carboxylated Ti6Al4V surface

To assess the biomolecule grafting on the carboxylated alloys surfaces, the spectra were compared to the chitosan standard one.

In this case, in the spectra of alloy samples, the main bands characteristic of the chitosan, were absent and the band at 1726 cm^{-1} of C=O stretching was present. It was evident that the reaction between the chitosan and the carboxyl groups on alloy surface did not take place.

To overcome this problem, we tried to immerse the same samples, for other 16 hours at room temperature in a solution of chitosan, EDC, NHS in MES buffer.

After the second immersion for 16 hours, the spectra (a), (b) and (c), in figure 4.8 of Ti6Al4V(A)_chitosan, Ti6Al4V(B)_chitosan and Ti6Al4V(C)_chitosan respectively, presented the characteristic peaks of chitosan.

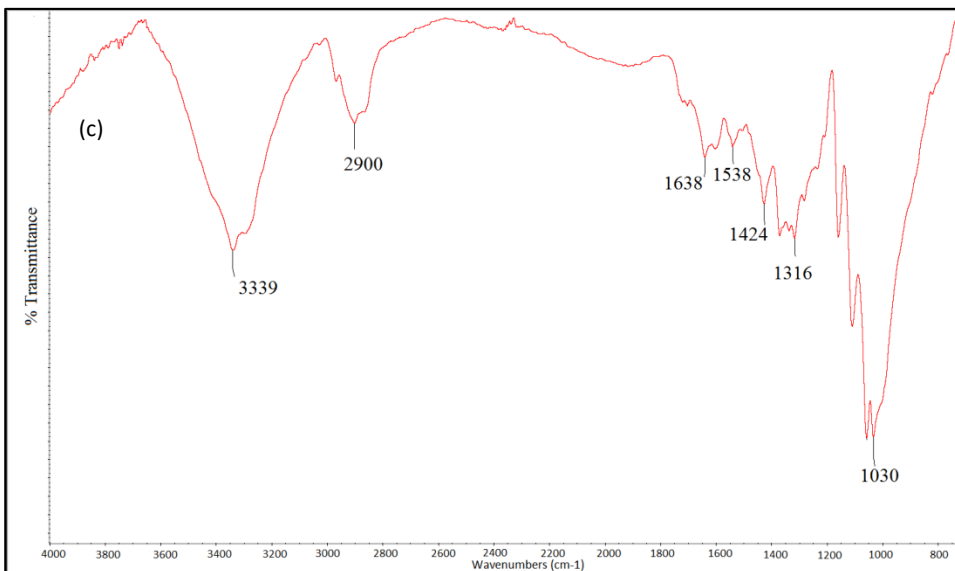
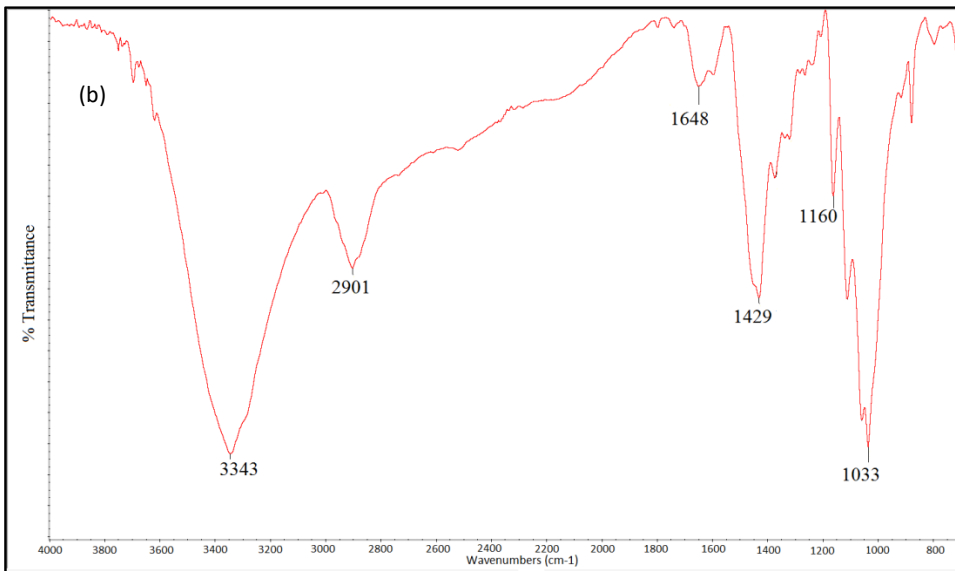
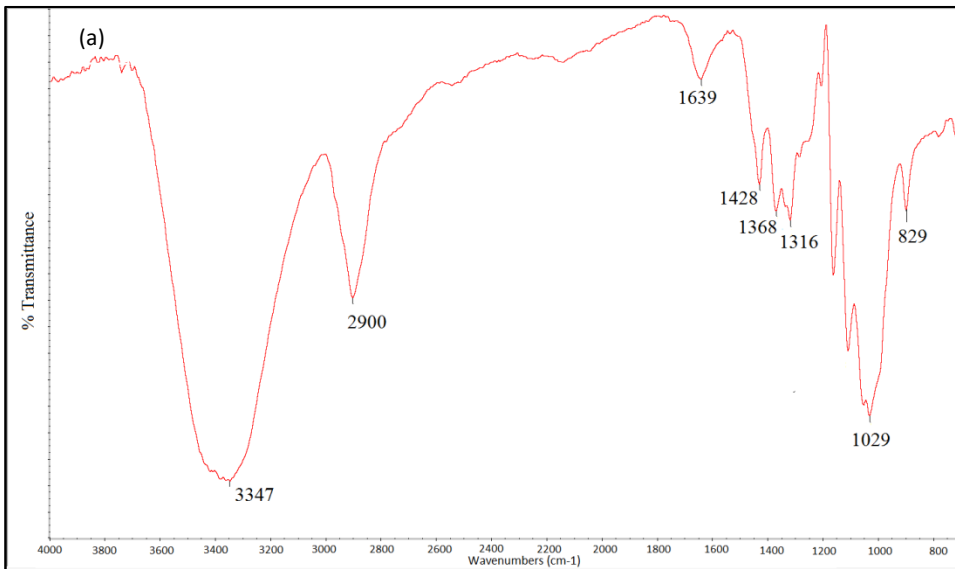


Figure 4.8: FTIR spectra, obtained after chitosan grafting procedure of untreated alloy (Ti6Al4V(A)_chitosan) (a), HCl pretreated alloy (Ti6Al4V(B)_chitosan) (b) and HF pretreated alloy (Ti6Al4V(C)_chitosan) (c).

When the substrate was Ti6Al4V alloy, a longer time of reaction between the substrate and the chitosan, than titanium surface was necessary. In this case, it was not possible to assess which is the pretreatment, that permitted the best functionalization of Ti6Al4V alloy with chitosan by only FTIR analysis. For a more detailed and quantitative description of surface chemistry, it was necessary to turn to XPS analysis for support.

4.3.3 X-ray Photoelectron Spectroscopy (XPS) analysis

XPS permits an accurate monitoring of surface changes and gives information on the chemical structure and the atomic concentration of different types of surface [9].

The chemical analysis of chitosan grafting on metal surfaces was supported by this technique, for a quantitative and detailed analysis.

The deconvoluted peaks of C1s of titanium and Ti6Al4V samples gave three peaks, as reported in table 4.2. Peaks at 285.0 eV, at 286.0 eV, at 288.0 eV were respectively assigned to C-C, C-O and O-C=O. Furthermore, in some samples, also a fourth component of deconvoluted C1s was present and it was related to spurious peaks, originated from the sample holder.

The deconvoluted peaks of O1s of all samples gave three signals too. These three peaks at 530 eV, at 532.2 eV and 534 eV were assigned to O-Ti and O-C signals and physisorbed water respectively. In particular the first one came from the metallic substrate surface; instead, the second one originated from the organic overlayer.

Other signals as N1s and Ti2p were analyzed, respectively relative to N, assigned to NH₂ or N-C=O and to Ti of substrate.

Signal	BE(eV)	Attribution
C1	285.0	C-C
C2	286.6	C-O
C3	288.7	O-C=O
O1	530.0	O-Ti
O2	532.2	O-C
O3	534.0	Physisorbed H ₂ O
N	400	NH ₂ , N-C=O
Ti	458	Ti

Table 4.2: Observed signals during measurements with their binding energy and attribution

4.4.3.1 Carboxylation and chitosan grafting on titanium surfaces

On the untreated titanium Ti(A), HCl pretreated titanium Ti(B) and HF pretreated titanium Ti(C), Ti2p, C1s and N1s analysis suggested a low organic material content, especially relative to surface contamination. The Ti/C intensity *ratio*, in detail, appeared almost identical in Ti(A), Ti(B) and Ti(C) samples. Instead, Ti/N appeared unusually greater in the starting HCl pretreated sample Ti(B), than in the untreated Ti(A) and HF pretreated Ti(C) samples, as shown in table 4.3.

Xu and co-workers reported it appeared difficult to remove physisorbed carbon and atmospheric nitrogen, this latter being considered as minor contamination on starting surfaces [10].

	Ti	Ti/C	C2/Ti	C3/Ti	N/Ti	O/Ti
Ti(A)	1686.33	0.33	0.72	0.35	0.069	2.13
Ti(A)_linker	1175.31	0.17	1.64	0.76	0.24	2.71
Ti(A)_chitosan	448.55	0.07	4.58	1.9	0.89	6.71
Ti(B)	1532.62	0.30	0.67	0.30	0.11	1.75
Ti(B)_linker	1652.66	0.26	0.99	0.39	0.11	1.86
Ti(B)_chitosan	1277.78	0.14	2.33	1.9	0.40	3.30
Ti(C)	1516.79	0.33	0.62	0.53	0.083	2.43
Ti(C)_linker	1156.25	0.15	1.36	0.83	0.16	2.06
Ti(C)_chitosan	819.43	0.14	2.04	1.04	0.35	4.39

Table 4.3: XPS Ti2p signal intensity and intensities ratio of elements analyzed for titanium samples.

After the carboxylation (step 1, fig. 4.1), in Ti(A)_linker, Ti(B)_linker, and Ti(C)_linker, the C1s peak intensity increased compared to the control samples Ti(A), Ti(B) and Ti(C) respectively as expected. Indeed, in table 4.3, the Ti/C *ratio* decreased and also the intensity of Ti signal.

In detail, an increase of C2 component was evident taking into consideration the C2/Ti *ratio* in table 4.3. The presence of carboxyl group was confirmed by the increase of the C3/Ti *ratio* if the samples of titanium and titanium with linker were compared. This trend suggested a very similar functionalization yield for the untreated titanium sample and for two acid etching pretreated samples.

For Ti(A)_linker, Ti(B)_linker, and Ti(C)_linker, the superficial presence of nitrogen was revealed, but its intensity was comparable with the relative starting samples one.

In the carboxylated titanium samples with chitosan grafting (step 2, fig.4.1), total C1s signal intensity increased, highlighted mostly with a decrease in the Ti/C signals *ratio*.

The chitosan is constituted of C1 and C2 components in 1:1 *ratio* and to confirm the chitosan grafting on carboxylated samples, it was convenient to analyze the atomic *ratios*, relative to C2, C3, N, O2+O3, considered as markers and titanium signal.

All titanium samples, the untreated Ti(A)_chitosan, and HCl and HF pretreated (Ti(B)_chitosan and Ti(C)_chitosan) showed a clear increase of the marker/titanium *ratios* compared to the carboxylated samples respectively. This increasing trend can be considered as a valid proof of the covalent grafting of the chitosan on the titanium substrates.

In the end, to characterize the organic layer, deposited on the Ti(A)_chitosan, Ti(B)_chitosan Ti(C)_chitosan, the N/C2 *ratio* was chosen as a signature of polysaccharide structure. This *ratio* was compared with a reference value, which was measured on a titanium foil covered by a chitosan powder. For all samples, the results suggested that the N/C2 obtained values were very close to the reference one, as shown in table 4.4. Therefore, the chitosan grafting on titanium samples formed a homogeneous layer on the surfaces. Analyzing this table, it was possible to suppose a better functionalization in the HCl and HF pretreated samples, since in these cases, the N/C2 *ratio* was 0.17, close to chitosan standard one 0.15.

	N/C2
Ti(A)_chitosan	0.19
Ti(B)_chitosan	0.17
Ti(C)_chitosan	0.17
chitosan	0.15

Table 4.4: Marker/Titanium signals ratio for chitosan grafting samples.

4.4.3.2 Carboxylation and chitosan grafting on Ti6Al4V surfaces

First, C1s and Ti2p signals were evaluated, as reported in table 4.5. The samples of the untreated Ti6Al4V(A), and pretreated with HCl and HF (Ti6Al4V(B) and Ti6Al4V(C) alloys were compared to the respectively samples obtained after carboxylation.

As shown in table 4.5, for sample of untreated alloy Ti6Al4V(A), an increase of Ti signal was observed and consequently an increase of the Ti/C *ratio*. This result was not according to the presence of –COOH groups on the surface after carboxylation, as it was detected by FTIR analysis. Probably, it was due to a high quantity of contamination organic material present on the starting sample despite the cleaning with acetone and ethanol. Indeed, also the *ratio* of C2/Ti and C3/Ti, reported in table 4.5, for these samples Ti6Al4V(A) and Ti6Al4V(A)_linker, confirmed this trend.

On the contrary, in Ti6Al4V(B)_linker and Ti6Al4V(C)_linker samples compared to Ti6Al4V(B) and Ti6Al4V(C) respectively, a decrease of Ti/C *ratio* was found and then an increase of C2/Ti and C3/Ti *ratio* was observed, as shown in table 4.5. In this case, XPS analysis confirmed that the carboxylation of pretreated with HCl and HF alloy samples took place. Probably, the acid etching of alloy surfaces allowed to obtain a clean starting surface.

	Ti	Ti/C	C2/Ti	C3/Ti	N/Ti	O/Ti
Ti6Al4V(A)	1448.83	0.16	1.78	1.03	0.59	3.36
Ti6Al4V(A)_linker	1528.84	0.24	0.86	0.47	0.0093	2.58
Ti6Al4V(A)_chitosan	873.32	0.089	3.59	1.45	0.44	4.8
Ti6Al4V(B)	1260.28	0.23	0.95	0.58	0.15	2.65
Ti6Al4V(B)_linker	1460.45	0.22	1.18	0.58	0.13	2.08
Ti6Al4V(B)_chitosan	178.37	0.025	10.78	5.2	1.43	20.2
Ti6Al4V(C)	2214.1	0.37	0.53	0.45	0.13	1.17
Ti6Al4V(C)_linker	2165.38	0.25	1.13	0.53	0.20	1.46
Ti6Al4V(C)_chitosan	1174.23	0.14	2.53	1.064	0.51	3.62

Table 4.5: XPS Ti2p signal intensity and intensities ratios of analyzed elements for alloy samples

In carboxylated alloys with chitosan grafting, a clear increase of total C1s signal intensity was revealed by a decrease of the C/Ti *ratio*, as shown in table 4.5. To confirm the chitosan grafting on the carboxylated alloys, in the same way of titanium foil, the atomic *ratios*, between the C2, C3, N, O2+O3 marker signals of chitosan and titanium signal respectively were analyzed. In all samples Ti6Al4V(A)_chitosan, Ti6Al4V(B)_chitosan Ti6Al4V(C)_chitosan, compared to the carboxylated samples respectively, a clear increase of markers/titanium *ratios* was observed.

In the end, to explore the distribution of the organic layer, on the Ti6Al4V(A)_chitosan, Ti6Al4V(B)_chitosan and Ti6Al4V(C)_chitosan, as for titanium samples, the N/C2 *ratio* was evaluated and compared to the reference one of chitosan value.

Analyzing the results in table 4.6, it was possible to assert a more homogeneous functionalization with chitosan, in the HCl sample, than the untreated and HF pretreated sample ones.

	N/C2
Ti6Al4V(A)_chitosan	0.12
Ti6Al4V(B)_chitosan	0.13
Ti6Al4V(C)_chitosan	0.20
chitosan	0.15

Table 4.6: Marker/Titanium signals ratio for grafted chitosan samples.

4.3.4 Electrochemical analysis: cyclic voltammetry

Cyclic voltammetry is the most widely used potentiostatic technique for acquiring qualitative information about electrochemical reactions. The power of cyclic voltammetry results from its ability to rapidly provide considerable information on the thermodynamics of redox processes.

It offers a rapid location of redox potentials of the electroactive species, and a convenient evaluation of the effect of media on the redox process.

Cyclic voltammetry consists of scanning linearly the potential of a stationary working electrode (in an unstirred solution), using a triangular potential waveform. During the potential sweep, the potentiostat measures the current resulting from the applied potential. The resulting current–potential plot is termed a cyclic voltammogram.

Among various applications of cyclic voltammetry as analytical method, it can be used to characterize the organic layer bonded to the proper substrate [11-12]. In this context, the electrochemical characterization of chitosan films deposited at a gold electrode by cyclic voltammetry was reported [13].

Unfortunately, the chitosan films are electrochemically inactive. In fact, cyclic voltammogram recorded at titanium electrode with chitosan grafting as Ti(A)_chitosan in a 0.1M KCl solution was comparable to the baseline obtained at the bare titanium electrode Ti(A) (fig 4.9, (a)).

No electrochemical signature of the polysaccharide film was observed between 0.90 V and -0.50 V for Ti(A)_chitosan.

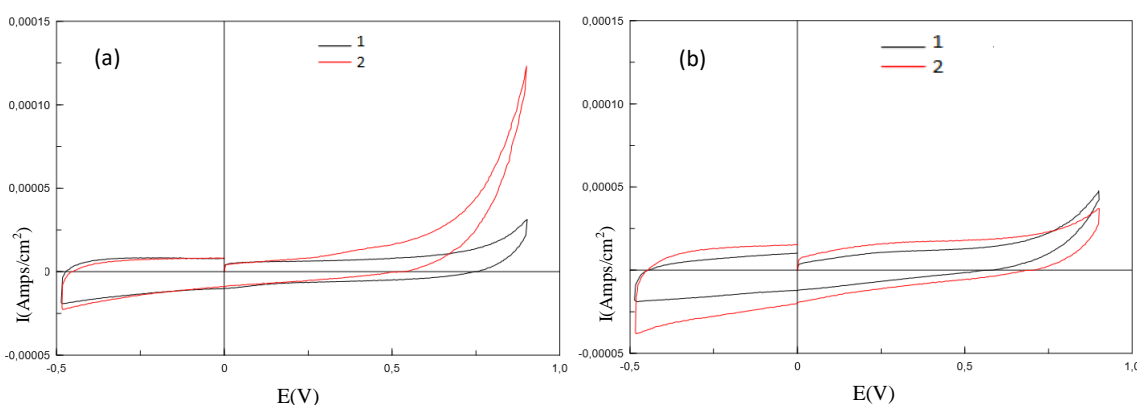


Figure 4.9: Cyclic voltammograms (0.05 V/s scan rate) in 0.1 M KCl at: (a) untreated titanium electrode, 1-Ti(A) and 2-Ti(A)_chitosan; (b) untreated titanium alloy electrode respectively, 1-Ti6Al4V(A) and 2-Ti6Al4V(A)_chitosan.

The same considerations can be asserted also for the alloy samples (4.9(b)).

The same results were obtained using titanium or titanium alloy pretreated with HCl or HF.

To evaluate the presence of chitosan grafting on the substrate, the same electrodes were then immersed in a solution containing the $\text{Fe}(\text{CN})_6^{3-/4-}$ redox couple. Indeed, as reported, an interaction between chitosan and this redox couple was observed [12, 13]. The electrochemical behaviour of the $\text{Fe}(\text{CN})_6^{3-/4-}$ redox couple was tested by cycling the potential of the working electrode in the same potential window of CV baseline, acquired before.

The voltammograms of $\text{Fe}(\text{CN})_6^{3-/4-}$ redox couple, recorded at the bare titanium electrode and the chitosan coated electrodes are shown in figures 4.10, respectively for the untreated(a), HCl(b) and HF(c) pretreated titanium samples.

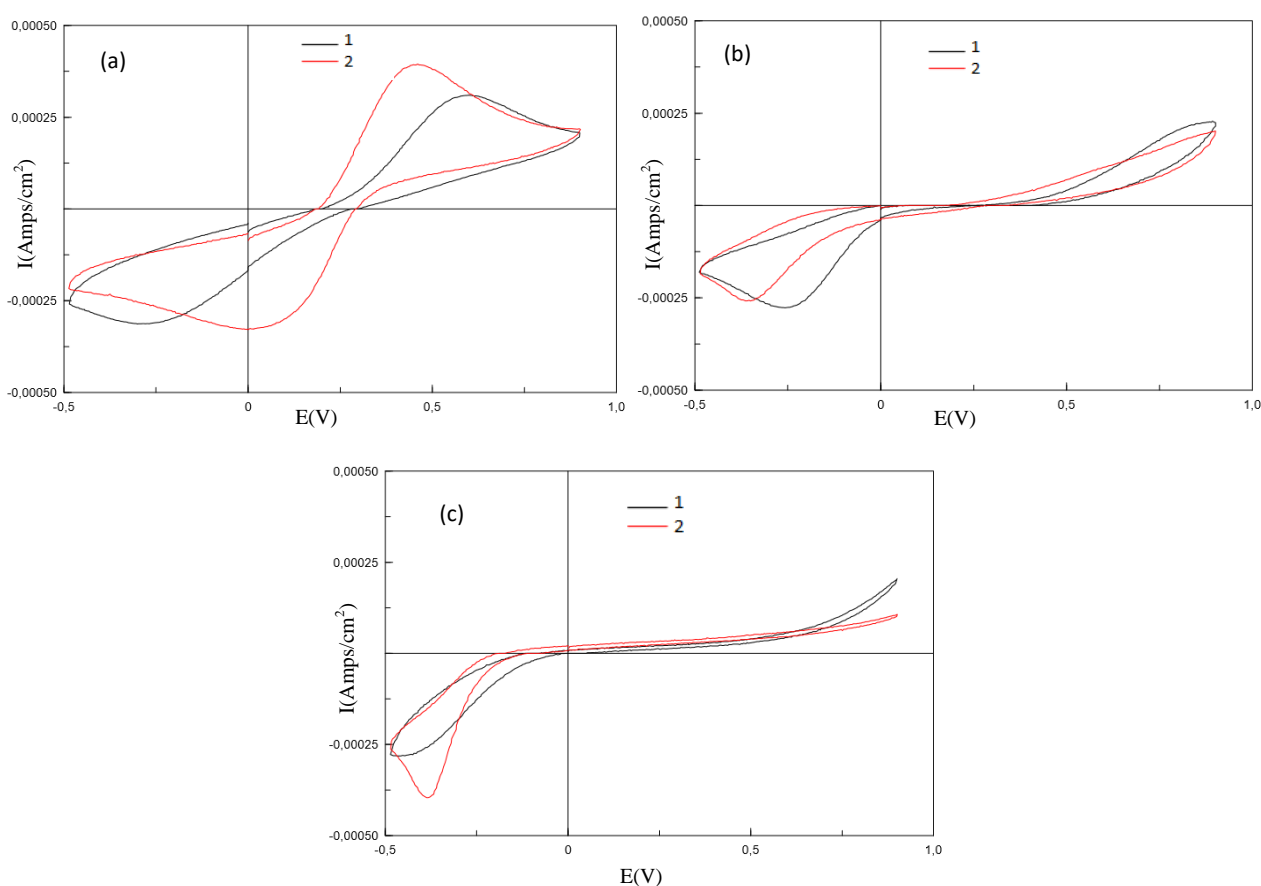


Figure 4.10: Cyclic voltammograms (0.05 V/s scan rate) in a 0.1 M KCl containing 1 mM of $\text{K}_3\text{Fe}(\text{CN})_6$ and 1mM of $\text{K}_4\text{Fe}(\text{CN})_6$ at: (a) untreated titanium electrode respectively, 1-Ti(A) and 2-Ti(A)_chitosan; (b) HCl pretreated titanium electrode respectively, 1-Ti(B) and 2-Ti(B)_chitosan; (c) HF pretreated titanium electrode respectively, 1-Ti(C) and 2-Ti(C)_chitosan.

As it can be seen the curves of titanium and chitosan coated titanium electrode were different. This was an additional proof of the presence of the chitosan and consequently the grafting of the polysaccharide on the surface.

In the same way, the voltammograms of $\text{Fe}(\text{CN})_6^{3-/4-}$ redox couple at the Ti6Al4V electrode and at the chitosan coated Ti6Al4V electrode are shown in figure 4.11, respectively for the untreated (a), HCl (b) and HF(c) pretreated alloy samples. The voltammograms at Ti6Al4V electrode and at chitosan coated Ti6Al4V electrode were different. Also in this case, cyclic voltammetry results confirmed the immobilization of chitosan on the substrates.

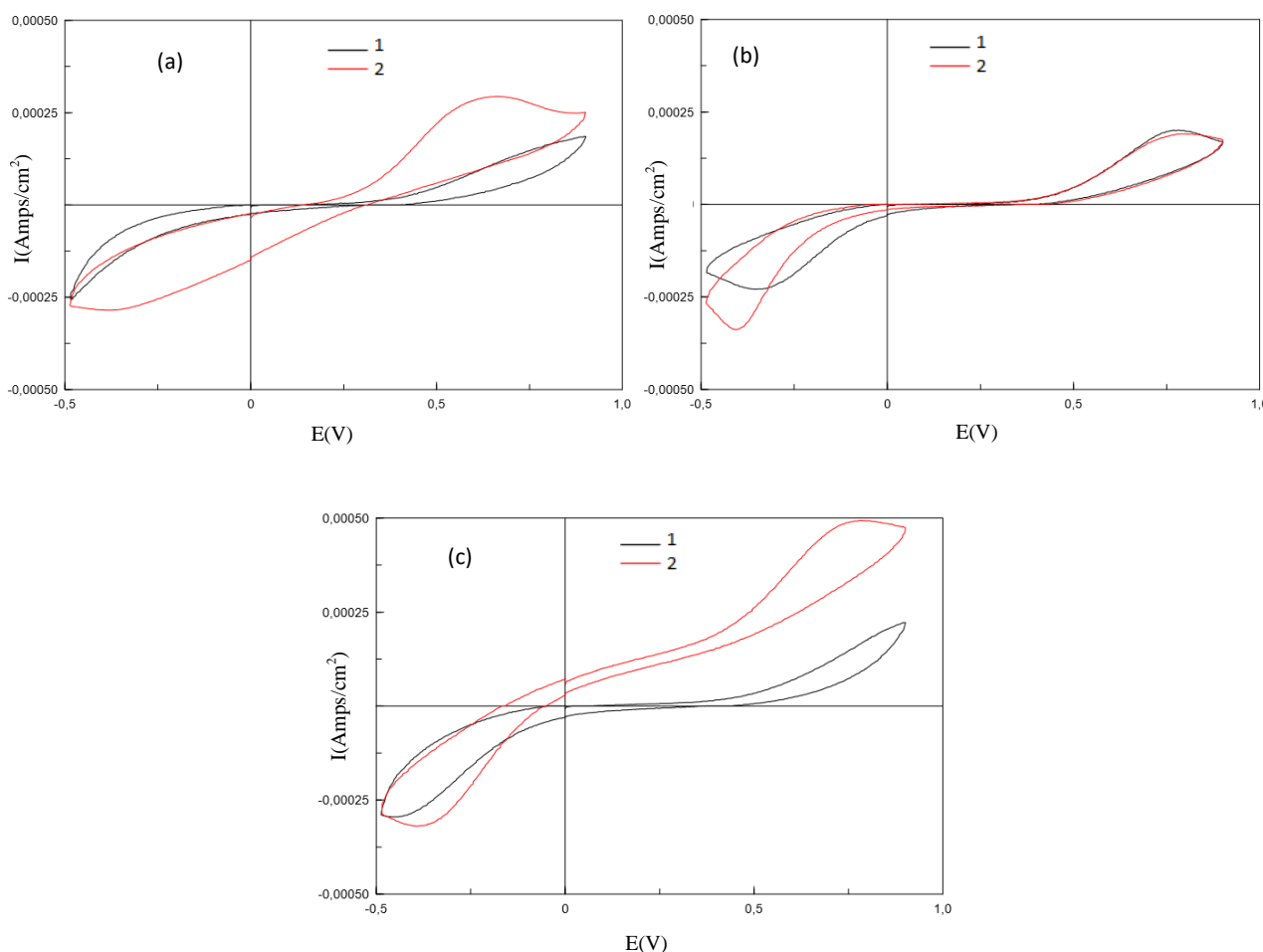


Figure 4.11: Cyclic voltammograms (0.05 V/s scan rate) in a 0.1 M KCl containing 1 mM of $\text{K}_3\text{Fe}(\text{CN})_6$ and 1mM of $\text{K}_4\text{Fe}(\text{CN})_6$ at: (a) untreated titanium alloy electrode respectively, 1-Ti6Al4V(A) and 2-Ti6Al4V(A)_chitosan; (b) HCl pretreated titanium alloy electrode respectively, 1-Ti6Al4V(B) and 2-Ti6Al4V(B)_chitosan; (c) HF pretreated titanium alloy electrode respectively, 1-Ti6Al4V(C) and 2-Ti6Al4V(C)_chitosan

The electrochemical analysis was used to evaluate the advantage of chitosan immobilization by covalent grafting using $-\text{COOH}$ as agent linker, compared to simple chitosan physisorption. For this analysis, the HCl pretreated titanium and Ti6Al4V alloy samples were chosen, because on these pretreated surfaces, the grafting of chitosan was resulted the best.

The voltammograms of the $\text{Fe}(\text{CN})_6^{3-/4-}$ redox couple in 0.1 M KCl solution recorded at Ti(B), Ti(B)_chitosan and Ti(B)_physis electrodes are reported in figure 4.12. As it can see the voltammogram at Ti(B)_physis electrode is similar to the curve at titanium electrode without chitosan Ti(B).

This result showed that probably on Ti(B)_physis sample, the interaction between the chitosan and the titanium surface was rather weak.

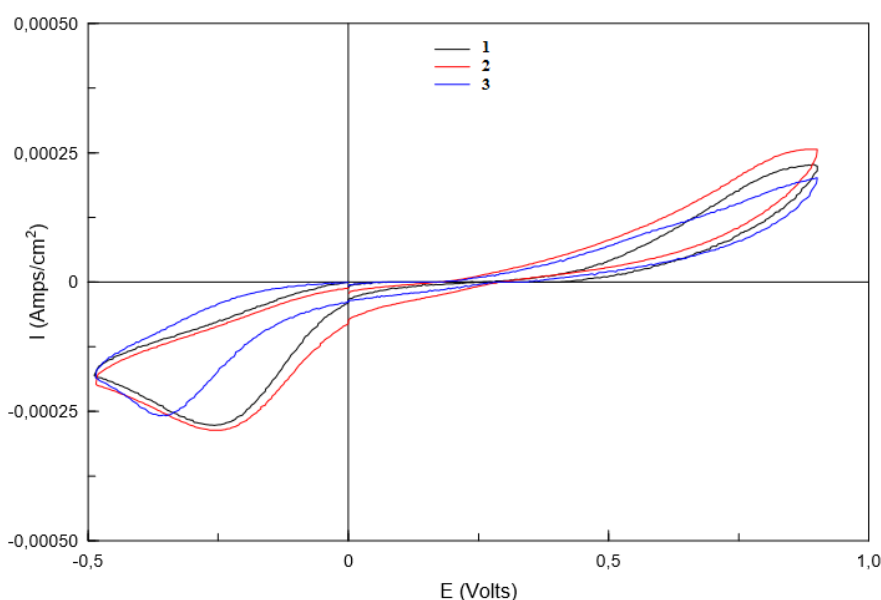


Figure 4.22: Cyclic voltammograms (0.05 V/s scan rate) in a 0.1 M KCl at containing 1 mM of $\text{K}_3\text{Fe}(\text{CN})_6$ and 1mM of $\text{K}_4\text{Fe}(\text{CN})_6$ at: 1- HCl pretreated titanium electrode; 2-chitosan physisorbed titanium electrode 3- chitosan covalently grafted titanium electrode

The same considerations could be asserted also for the alloy samples. As shown in figure 4.13, the voltammograms at Ti6Al4V(B) (1) and Ti6Al4V(B)_physis (2) were similar. Therefore, on HCl pretreated titanium and on titanium alloy, to obtain a stable immobilization of chitosan, it was fundamental the use of carboxyl group to covalently bond the chitosan on the surface.

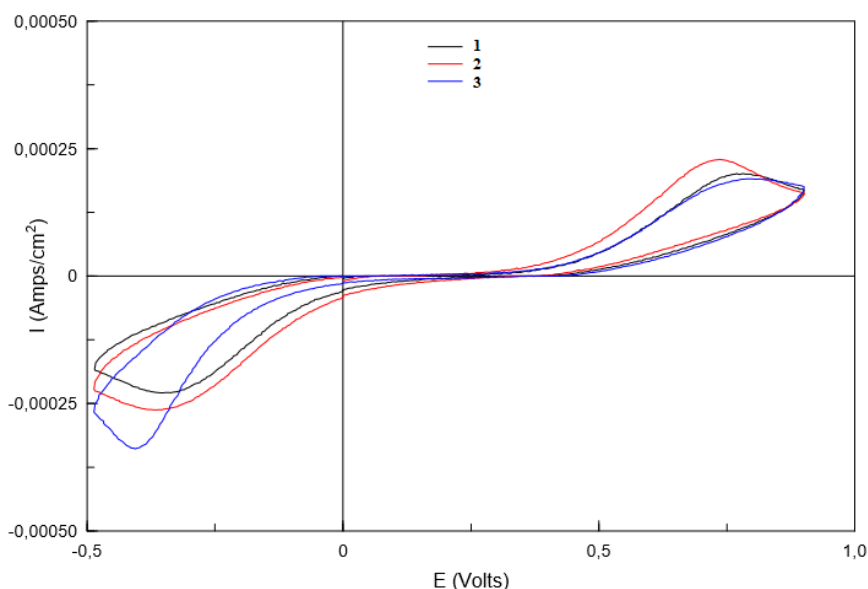


Figure 4.13: Cyclic voltammograms (0.05 V/s scan rate) in a 0.1 M KCl at containing 1 mM of $K_3Fe(CN)_6$ and 1mM of $K_4Fe(CN)_6$ at: 1- HCl pretreated Ti6Al4V electrode; 2- chitosan physisorbed Ti6Al4V electrode; 3- chitosan covalently grafted Ti6Al4V electrode.

4.4 Conclusions

In order to simplify and to optimise the way to bond chitosan on the titanium surface, in this study, a new easy procedure was proposed, employing the carboxyl group as linker agent to graft the chitosan on titanium and Ti6Al4V alloy.

Different pretreatments of the surface were investigated to study the influence on the performance of the subsequent grafting of chitosan. The effect of these pretreatments on titanium and Ti6Al4V surfaces was analysed by SEM images.

The characterization of all titanium and Ti6Al4V alloy surfaces, after carboxylation with chloroacetic acid and subsequent grafting with chitosan was performed by FTIR and XPS analysis. These techniques, showed the presence of $-COOH$ groups after carboxylation and the covalent immobilization of chitosan on the untreated, HCl and HF pretreated titanium or Ti6Al4V surfaces. In correspondence of HCl etched samples the formation of a homogeneous film of chitosan was observed. This result is hopeful, for the future in vitro cell tests, because it's demonstrated that a rough surface, as the one obtained after HCl etching, would enhance cell adhesion properties.

Finally, it could possible to assert that the cyclic voltammetry was a valid tool to electrochemical check the immobilization of chitosan on titanium and Ti6Al4V alloy surface. Furthermore, by this

analysis, it was proved the importance of carboxyl groups to immobilize covalently and stably chitosan on metal surfaces.

4.5 References

- [1] A. Nanci, J.D. Wuest, L. Peru, P. Brunet, V. Sharma, S.ZAlzai, M.D. McKee. Chemical modification of titanium surfaces for covalent attachment of biological molecules. *Journal of Biomedical Materials Research*, 40(2):324-35, 1998
- [2] B. Rajaeian, A. Heitz, M.O. Tade, S. Liu. Improved separation and antifouling performance of PVA thin film nanocomposite membranes incorporated with carboxylated TiO₂ nanoparticles. *Journal of Membrane Science* 485:48-59, 2015
- [3] Z. Shi, K.G. Neoh, E.T. Kang, C.K. Poh, W. Wang. Surface Functionalization of titanium with carboxymethyl chitosan and immobilized bone morphogenetic protein-2 for enhanced osseointegration. *Biomacromolecules* 10:1603-1611, 2009
- [4] NIST X-ray Photoelectron Spectroscopy Database, Version 4.1 (National Institute of Standards and Technology, Gaithersburg, 2012
- [5] A Smargiassi, J. Bertacchini, M. Checchi, F. Cavani, M. Ferretti and C. Palumbo. Biocompatibility Analyses of Al₂O₃-Treated Titanium Plates Tested with Osteocyte and Fibroblast Cell Lines. *Biomedicines*, 32,5(2), 2017
- [6] E. Petrucci, D. Montanaro, M. Orsini and G. Sotgiu. Micro- and nanostructured TiO₂ substrate: Influence on the electrocatalytic properties of manganese oxide based electrodes. *Journal of Electroanalytical Chemistry*, 2017
- [7] Hua-Cai Ge, D.K Luo. Preparation of carboxymethyl chitosan in aqueous solution under microwave irradiation. *Carbohydrate Research*, 340, 1351-1356, 2005
- [8] W. Chen, X. Shen, Y. Hu, K. Xu, Q. Ran, Y. Yu, L. Dai, Z. Yuan, L. Huang, T. Shen, K. Cai. Surface functionalization of titanium implants with chitosan-catechol conjugate for suppression of ROS-induced cells damage and improvement of osteogenesis, *Biomaterials*, 114, 82-96, 2017
- [9] M. D'Almeida, J. Amalric, C. Brunon, B. Grosogeat, B. Toury. Relevant insight of surface characterization techniques to study covalent grafting of a biopolymer to titanium implant and its acidic resistance. *Applied Surface Science*, 327, 296-306, 2015

- [10] X. Xu, L. Wang, S. Guo, L. Lei, & T. Tang. Surface chemical study on the covalent attachment of hydroxypropyltrimethyl ammonium chloride chitosan to titanium surfaces. *Applied Surface Science*, 257(24), 10520-10528, 2011
- [11] J. Pinson, F. Podvorica. Attachment of organic layers to conductive or semiconductive surfaces by reduction of diazonium salts. *The Royal Society of Chemistry*, 34, 429-439, 2005
- [12] P. E. Canavar, E. Eksin, A. Erdem. Electrochemical monitoring of the interaction between mitomycin C and DNA at chitosan carbon nanotube composite modified electrode. *Turkish Journal of Chemistry*, 39, 1-12, 2005
- [13] R.A. Zangmeister, J.J. Park, G. Rubloff, M. J. Tarlov. Electrochemical study of chitosan films deposited from solution at reducing potentials. *Electrochimica Acta*, 51, 5324-5333, 2006

Chapter 5

Conclusions

In this work, the covalent immobilization of biomolecules, as lactose modified chitosan and chitosan, on poly(ϵ -caprolactone), titanium and Ti6Al4V alloy was achieved with good results both for polymeric surface and for metal surfaces.

A novel functionalization of poly(ϵ -caprolactone), a polyester used to produce applicable *in vivo* scaffolds for bone, cartilage, ligaments and tendons, was obtained. The PCL surface was undergone to alkaline hydrolysis to increase the content of the carboxyl groups, for the further grafting with two different lactose-modified chitosan (chitlac A and chitlac B). ToF-SIMS and univariate and multivariate statistical analysis were used in synergy to characterize the surface chemistry. The results showed the formation of a homogeneous layer of chitlac on the hydrolyzed PCL and also suggested a greater grafting degree of hydrolyzed PCL membrane when chitlacB was used as grafting agent.

A new and simple functionalization of titanium and Ti6Al4V alloy was obtained by covalent grafting of chitosan, to improve antibacterial properties. In detail, different pretreatments of the surface were studied, to identify the one which permits the highest functionalization yield. By FTIR and XPS analysis of metal surfaces, the presence of $-\text{COOH}$ group after carboxylation with chloroacetic acid, was confirmed. Furthermore, the grafting of chitosan on carboxylated surfaces was proved with good results. Moreover the cyclic voltammetric analysis confirmed the chitosan grafting on the metal surfaces and permitted to affirm that the presence of carboxyl groups was fundamental for chitosan immobilization. The best superficial pretreatment was the HCl etching. This result was desired, because it's demonstrated that a rough surface enhances cell adhesion properties.

Future developments will be, both for PCL and titanium, to test *in vitro* the functionalized surfaces, in terms of antibacterial properties and cell interactions.

Furthermore, future challenges could be oriented towards the exportation of the applied strategies to graft a large variety of bioactive molecules on PCL and carboxylated titanium and Ti6Al4V alloy surfaces.